MICROFLUIDIC-BASED FABRICATION OF MICROGELS FOR TISSUE ENGINEERING

by

Roya Samanipour

BSC., (Mechanical Engineering) Chamran University, Iran. 2008
MSC., (Mechanical Engineering) Tarbiat Modares University, Iran. 2012

A THESIS SUBMITTED IN PARTIAL FULFILLMENT OF
THE REQUIREMENTS FOR THE DEGREE OF

Master of Science

in

THE COLLEGE OF GRADUATE STUDIES

(Interdisciplinary Studies)

THE UNIVERSITY OF BRITISH COLUMBIA

(Okanagan)

February 2016

a place of mind
THE UNIVERSITY OF BRITISH COLUMBIA

The College of Graduate Studies

The undersigned certify that they have read, and recommend to the College of Graduate Studies for acceptance, a thesis entitled:

Microfluidic – based Fabrication of Microgels for Tissue Engineering.

submitted by Roya Samanipour in partial fulfilment of the requirements of

the degree of Master of Science in Interdisciplinary Studies.

Dr. Keekyoung Kim / Mechanical Engineering

Supervisor, Professor (please print name and faculty/school above the line)

Dr. Mina Hoorfar / Mechanical Engineering

Supervisory Committee Member, Professor (please print name and faculty/school in the line above)

Dr. Frederic Menard / Chemistry

Supervisory Committee Member, Professor (please print name and faculty/school in the line above)

Dr. Liwei Wang / Mechanical Engineering

University Examiner, Professor (please print name and faculty/school in the line above)

External Examiner, Professor (please print name and university in the line above)

January 20, 2016

(Date Submitted to Grad Studies)

Additional Committee Members include:

(please print name and faculty/school in the line above)

(please print name and faculty/school in the line above)

Abstract

This thesis presents the experimental and computational study of hydrogel microgels using flow-focusing devices. The microfluidic devices were fabricated to generate microgels from two immiscible phases of fluids. Conventional replica molding and photolithography methods were used to fabricate a rectangular channel microfluidic device. Using the flow-focusing microfluidic devices, effects of various parameters on hydrogel pre-polymer droplet generation were investigated experimentally and computationally. First, three-dimensional (3D) computational simulations were conducted to study the physics of hydrogel pre-polymer droplet formation mechanism in three different regimes: squeezing, dripping, and jetting regime. Subsequently, effects of viscous, inertia and surface tension force on the gelatin methacrylate (GelMA) pre-polymer droplet generation and droplet size were studied through experiments. Finally, based on computational and experimental results, the uniformly controlled size of GelMA microgels was created. All experimental data were summarized by a capillary number of the dispersed and the continuous phases to characterize the different regimes of GelMA pre-polymer droplet generation and to predict the transition of dripping to a jetting regime for GelMA pre-polymer in the flow-focusing device. Also, two types of cells, MCF-7 breast cancer cells, and 3T3 fibroblasts, were mixed in a 5 wt% GelMA pre-polymer solution used as dispersed phase. The uniform cell-laden GelMA microgels were fabricated and the cell viability was over 80%. In addition, a new method to create the polydimethylsiloxane (PDMS) circular channel was developed using a rapid and cheap 3D printing process. Due to the resolution limitation of 3D printing, the channels were elliptical, and subsequent liquid PDMS injection process was adopted to form fully circular channels.

Preface

The research presented in this thesis is the original work of the author. The research was conducted under the supervision of Dr. Keekyoung Kim at the Integrated Bio-Micro/Nanotechnology Laboratory in the School of Engineering at UBC Okanagan. Parts of this thesis have been published in peer reviewed scientific journals and conference proceedings, and my supervisor is the co-authors of all of the publications.

Contribution

The results of this thesis have been partially published in peer-reviewed journals and conferences. The detail of the author contributions is as follow,

Chapter 1 is based on the published journal paper. Z. Wang*****, **R. Samanipour***, K. Koo, and K. Kim, "Organ-on-a-chip platforms for drug delivery and cell characterization: a review," *Sensors and Materials*, vol. 27, no. 6, 487-506, 2015. I wrote half of the review paper and Dr. Kim took care of the final edition and submission.

Chapter 3 is based on the paper which is under review. **R. Samanipour**, Z. Wang, A. Ahmadi, and K. Kim, **"**Computational and experimental study of the microfluidic flow-focusing generation of hydrogel droplets," *Journal of Applied Polymer Sciences*, minor revision, 2015. I developed the numerical model of droplet generation and wrote the paper and Dr. Kim took care of the final edition and submission.

Chapter 4 is based on the paper which is under review. **R. Samanipour**, Z. Wang, A. Ahmadi, and K. Kim, **"**Computational and experimental study of the microfluidic flow-focusing generation of hydrogel droplets," *Journal of Applied Polymer Sciences*, minor revision, 2015. I have done all the lab work and data analysis and Dr. Kim took care of the final edition and submission.

Chapter 5 is based on the published paper. B. Parker*****, **R. Samanipour***, A. Ahmadi, and K. Kim, "Fabrication of circular channel microfluidic chips using post-processed 3D printing and PDMS injection for droplet generation," *Micro and Nano Letters*, published online, DOI: 10.1049/mnl.2015.0329, 2015. I have done all the lab work and Dr. Kim took care of the final edition and submission.

Article published or accepted in refereed journals (* equal contribution):

1. **R. Samanipour**, Z. Wang, A. Ahmadi, and K. Kim, **"**Computational and experimental study of microfluidic flow-focusing generation of hydrogel droplets," *Journal of Applied Polymer Sciences*, under review, 2015.
2. R. Dai, Z. Wang, **R. Samanipour**, and K. Kim, "Adipose derived stem cells in tissue engineering," *Stem Cells International*, DOI: 10.1155/2016/6737345, 2016.
3. B. Parker*****, **R. Samanipour***, A. Ahmadi, and K. Kim, "Fabrication of circular channel microfluidic chips using post-processed 3D printing and PDMS injection for droplet generation," *Micro and Nano Letters*, published online, DOI: 10.1049/mnl.2015.0329, 2015.
4. Z. Wang*****, **R. Samanipour***, and K. Kim, "The cleanroom-free rapid fabrication of a liquid conductivity sensor for surface water quality monitoring," *Microsystem Technologies*, published online, DOI: 10.1007/s00542-015-2544-1, 2015.
5. Z. Wang*****, **R. Samanipour***, K. Koo, and K. Kim, "Organ-on-a-chip platforms for drug delivery and cell characterization: a review," *Sensors and Materials*, vol. 27, no. 6, 487-506, 2015.
6. Z. Wang, R. Abdulla, B. Parker, **R. Samanipour**, S. Ghosh, and K. Kim, "A simple and high-resolution stereolithography-based 3D bioprinting system using visible light crosslinkable bioinks," *Biofabrication*, published online, DOI: 10.1088/1758-5090/7/4/045009, 2015.

Other refereed contributions:

7. H. Nejad, **R. Samanipour,** Z. Wang, K. Kim, and M. Hoofar, "Cell-Patterning and culturing on digital microfluidics," *MicroTAS 2015*, Gyeongju, Korea, Oct. 2015.
8. A. Gupta, B. A. Nestor, M. D. de L. Derby, A. V. den Berg, **R. Samanipour**, Z. Wang, H. R. Nejad, K. Kim, M. Hoorfar, "3D cell patterning using dielectrophoresis on digital microfluidics," *IEEE EMBC 2015*, Milano, Italy, Aug. 2015.
9. Z. Wang, R. Abdulla, B. Parker, **R. Samanipour**, S. Ghosh, and K. Kim, "A high-resolution stereolithography system for 3D bio-printing application," *Canada-Korea Conference on Science & Technology (CKC 2015)*, Calgary, Alberta, Canada, Jul. 2015.
10. **R. Samanipour**, K. Kim, "Computational and Experimental study of microfluidic flow-focusing devices for synthesizing hydrogel microtissues," *ASME International Mechanical Engineering Congress & Exposition*, Montreal, Quebec, Canada, Nov. 2014.

Table of Contents

List of Tables

List of Figures

Acknowledgements

In the first place, I would like to thank my supervisor, Dr. Keekyoung Kim, for his guidance and expertise throughout graduate endeavors. He has been an invaluable source of inspiration and encouragement.

I would also like to thank my committee members and all of my other educators throughout the years whom I have learned from immensely, as well as my colleagues whom I have enjoyed working alongside in the lab.

I would like to thank my family for their continuous love and support. I am forever grateful for their generous time and compassion.

Lastly, I would like to thank my partner for being there every step along the way. The journey would not have been the same without you. Words cannot describe my appreciation for his endless insight.

Dedication

This thesis is dedicated to my beloved mother, Farideh Aflaki. It is impossible to thank her adequately for everything she has done for me, from raising me to loving me unconditionally. I truly want her to know that I love her very much deep in my heart.

Chapter 1 Introduction

Tissue engineering aims to create, repair, or replace biologically functional tissues using a combination of material, mechanical, chemical and biological sciences [1]. In tissue engineering, cells isolated from the biopsied tissues are encapsulated in biodegradable materials (e.g., hydrogels), where cells can be protected from outside environments to maintain their cellular function. Encapsulated cells can be further proliferated in biomimetic structures (scaffolds) which resemble cellular microenvironments. By transplanting the resulting construct into the patients' body, the scaffold will be degraded over time to form a new tissue [2]. During the transplantation, cells encapsulated in hydrogel scaffolds can be prevented from outside environments. The transplantation of cell-laden hydrogel was first used in 1964 to minimize immune rejection of transplanted cells [3]. Since then, several innovative methods have been developed to advance the area of tissue engineering. Despite the advances, there are still some limitations to control precisely the cellular microenvironment [4] and fabricate vascularized complex tissue structures [5].

1.1 Microscale Tissue Engineering

Microfabrication techniques have been developed as a powerful tool to overcome a number of tissue engineering challenges [6][7]. The ability to engineer the size and shape of hydrogel scaffolds using microfabrication techniques has opened new opportunities to address the challenges such as complex tissue architecture and vascularization [8]. Microfabrication techniques, such as photolithography, micromolding, and microfluidic fabrication, have been used to fabricate micrometer-sized hydrogels for encapsulating cells in micro structures [6][9]. In photolithography technique, a thin layer of photocrosslinkable hydrogel pre-polymer solution is exposed to a UV light through a

photomask. The area exposed to the UV light is polymerized and becomes a gel. This technique can be used to fabricate microstructures of hydrogels in a wide range of sizes from micrometers to millimeters. The micromolding technique is to fabricate engineered microtissue structures using a microfabricated mold. The hydrogels pre-polymer can be cast and crosslinked to fabricate a variety of microstructures. Another technique to fabricate hydrogel microstructures is the microfluidic technique which is a powerful method to generate well-controlled hydrogel droplets in a high-throughput way. Fluid properties within microfluidic channels can be easily modulated and generate hydrogels with controlled environments [6].

The microfluidic technique-based cell encapsulation has been widely used in recent years due to many advantages in comparison with other microfabrication techniques [6]. The microfluidic techniques offer the ability of a high-throughput generation of well-controlled monodisperse micrometer-sized spherical or rounded microgels, as well as hollow cylindrical gel fibers that cannot be created with other microfabrication techniques [8]. The size of droplets could be easily controlled by adjusting the flow rates of fluids and fluid properties such as viscosity and interfacial tension [10]. The microfluidic techniques also offer a high degree of control over the encapsulation process to get the desired number of cells per particles and spatial organization [11]. Controlling droplet size and fabricating small droplets (< 150 μm) can benefit the delivery of nutrients and oxygen to encapsulated cells in microgels. The microgels created in microfluidic devices can be used as building blocks of tissue structures [12]. For example, microgels containing different types of cells are assembled into a desired 3D structure to create functional tissues. A successful assembly process requires precisely controlling the size of the microgels. The microgels can be also used as a 3D cell culturing platform to study stem cell differentiation, cell-cell interaction, and cell-microenvironment interaction

[13][14]. The study of cell co-culture and cell fate regarding neighbor cells and the surrounding environment is also benefited from controlling the size of droplets and encapsulating various cells in each microgel [15]. The study of microenvironmental parameters (e.g., porosity and stiffness for cancer cell migration) is very crucial in tissue engineering due to their effect on cell response and fate [16]. The cell fate is influenced by microenvironmental parameters such as interaction with other cells, exposure to growth factors, mechanical stimuli, and shear forces [17]. Therefore, the microscale tissue engineering has many advantages over the conventional macroscale tissue engineering to modulate precisely the cell microenvironmental parameters to enhance the controllability of cell behavior. This study adopted microfluidic techniques to generate microgels for microscale tissue engineering applications.

1.2 Hydrogel Biomaterials

The properties of hydrogels used for cell encapsulation resemble extracellular matrix (ECM) in native tissues [18]. Hydrogels have been extensively used for a variety of tissue engineering applications in recent years due to their unique characteristics [19][20][21]. For examples, hydrogels form hydrophilic polymeric networks that can absorb the high volume of water without dissolving. They have native tissue-like elastic properties and biocompatibility [18]. The porous structure of hydrogels allows cells to attach to their microstructure, receive oxygen and nutrients, and release metabolic products to the surrounding environment.

There are two different types of hydrogels: synthetic (synthesized in a laboratory) and natural (obtained from natural resources) hydrogels [22]. Both synthetic and natural hydrogels are widely used in tissue engineering applications because of their biocompatibility and porous structures. The natural hydrogels are generally categorized into two main types; protein-based hydrogel (e.g., gelatin, collagen, hyaluronic acid, and

fibrin) and polysaccharides-based hydrogel (e.g., alginate, chitosan, and agarose) [22]. These natural hydrogels form networks via physical or ionic interactions. Synthetic hydrogels consisted of poly (ethylene glycol), poly (acrylic acid), and poly (vinyl alcohol) are synthesized by a radical chain or step-growth polymerization reaction [23]. Different hydrogels have different characteristics based on the polymerization methods and their structures which affect the cellular functions such as growth, differentiation, and migration of encapsulated cells. Each type of hydrogels has advantages and disadvantages in tissue engineering applications [18]. Natural hydrogels are inherently biocompatible and resemble native ECM. Therefore, they can interact with cells easily and promote various cellular functions. However, special processes are required to extract natural hydrogels from biological tissue, and the extracted volume is limited. On the contrary, synthetic hydrogels have limited cell-gel interaction in comparison to natural hydrogels. However, synthetic hydrogels are highly reproducible and readily available, and their composition can be controlled as needed for different cell lines.

In order to encapsulate cells, the pre-polymer solutions of both synthetic and natural hydrogels are first prepared and then crosslinked to become hydrogel scaffolds with cells. Crosslinking methods vary based on types of hydrogels. Radical polymerization can be done by heat, light or redox reactions [24]. Photocrosslinkable hydrogels such as polyethylene glycol and gelatin methacrylate are crosslinked by exposing them to a light. Temperature changes also crosslink hydrogels such as agarose and divalent ion crosslinks hydrogels such as alginate with Ca^{2+} [25]. Among them, photocrosslinkable hydrogels are most widely used in the microscale tissue engineering with the advantage of controlling crosslinking times. During photocrosslinking process, UV light disassociates photoinitiator molecules mixed with hydrogel pre-polymers into free radicals to induce the crosslinking of hydrogel networks [24]. However, the photocrosslinking process has

the risk that unreacted free radicals can also react with cellular components such as cell membranes, ECM proteins, and DNA [24]. This may result in low cell viability or the malignant transformation of cells exposed to UV. This risk factor can be reduced by washing the crosslinked hydrogels immediately with PBS several times to remove unreacted photoinitiators.

In the ideal tissue regeneration process, hydrogels are degraded over time and cells replace scaffolding structures with ECM. Therefore, degradability is particularly important for hydrogels used in tissue engineering applications. In the degradation process, the hydrophilic backbone of polymer chains is broken down due to enzyme activities [26][27]. The multi-functional crosslinking molecules can provide a wider range and tighter control over the degradation rates and mechanical stiffness of hydrogels [28]. Natural hydrogels, such as collagen, gelatin, fibrin, and chitosan, are biodegradable. Also, a synthetic nondegradable hydrogels, such as polyvinyl alcohol and polyethylene glycol, can be degradable by adding ester or peptide functional groups in the crosslinking agents [28].

1.3 Microfluidic Generation of Droplets

Aqueous monodisperse droplets are generated in a variety of microfluidic device configurations such as T-junction [29], flow-focusing [30], and co-axial [31] devices (Figure 1.1).

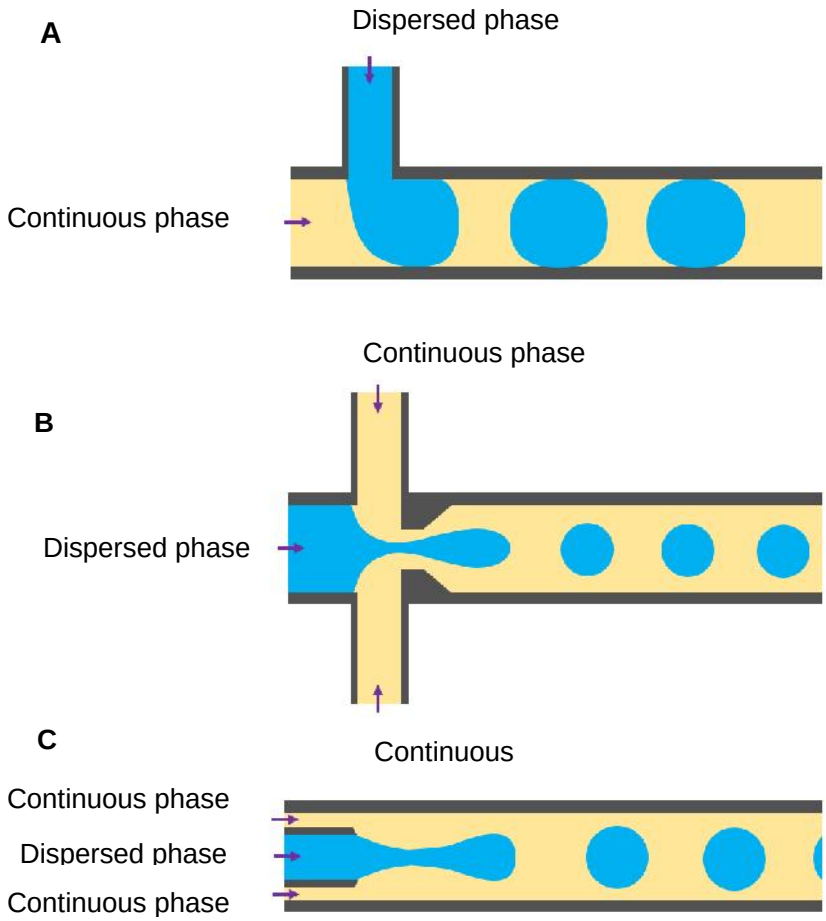

Figure 1.1 Schematic of microfluidic configurations for droplet generation. (A) T-junction microfluidic configuration. (B) Flow-focusing microfluidic configuration. (C) Co-flow microfluidic configuration.

These microfluidic methods can generate monodisperse uniform hydrogel droplets in a high throughput way. It is also possible to fabricate two or three emulsion droplets by arranging microfluidic channels in parallel [32][33]. Based on the required droplet frequency, droplet size, and droplet uniformity, the microfluidic devices with various configurations are used for generating droplets [34]. In a microfluidic device, a hydrogel pre-polymer solution mixed with cells as a dispersed phase is entered into a central inlet while a continuous phase fluid is entered into another inlet and surrounds the hydrogel

pre-polymer solution to form droplets (Figure 1.1). Nonpolar liquids, such as mineral, fluorinated, and vegetable oil, are usually used for the continuous phase [35][36][37]. In the flow-focusing (Figure 1.1B) and co-flow devices (Figure 1.1C), droplets break up when the viscous force of the continuous phase fluid overcomes the interfacial force that keeps droplets connected to the disperse phase fluid. To reduce surface energy, prevent coalescence, and increase monodispersity, surfactants (e.g., span 80, tween 20) are added to the continues phase fluid [34][15][38].

1.3.1 T-junction Configuration

T-junction microfluidic devices are widely used for droplet generation due to their simple fabrication steps and operation process [34]. In the T-junction configuration, the dispersed phase and continuous phase enter into two channels arranged in a perpendicular direction as shown in Figure 1.1A. The continuous phase meets and pushes the dispersed phase at the junction. The shear force and pressure gradient generated by the continuous phase fluid make a thin neck of the dispersed phase and finally creates a droplet. The size of droplets depends on the flow rate and viscosity of the dispersed and continuous phase fluids, as well as the geometry of microchannels. Several researchers have used T-junction microfluidic devices to encapsulate cells in microgels and studied the behavior of encapsulated cells. Kumachev *et al.* studied the effect of the elasticity of cellular microenvironments on cell fate by fabricating microgels with different elastic properties [39]. Tan *et al.* generated alginate particles with narrow size distribution using a new method combined with the internal gelation method [37]. In this study, the calcium carbonate nanoparticles mixed in the alginate solution induced the internal crosslinking. Droplets formed at the T-junction were broken off by a corn oil fluid. Lectin and acetic acid in the corn oil diffused into the droplets to crosslink them. Um et al. developed the T-junction microfluidic device with three different inlets for generating cell-laden

hydrogel beads [40]. In this device, pre-polymer solution entered into the first inlet and the oil phase containing surfactant entered into the second inlet to cut off the pre-polymer solution and generate droplets. Afterward, at the downstream of the channel, another liquid, which carries crosslinking materials, was injected into the third inlet to mix with the droplets. In another study of T-junction device, alginate pre-polymer and $CaCl_2$ solutions were used as dispersed phases while hexadecane was used as a continuous phase to fabricate the alginate droplets [41]. Alginate pre-polymer, $CaCl_2$, hexadecane entering from three different inlets were met at the junction to form a droplet and crosslinked by chaotic mixing in a microfluidic device.

1.3.2 Co-flow Glass Capillary Configuration

Co-flow devices consist of two glass capillaries−an inner glass capillary and outer glass capillary. Two fluid phases flow in the same direction in the glass capillaries. The dispersed phase fluid flows into the inner glass capillary. The continuous phase fluid flows into the outer capillary surrounding the inner capillary in the same direction, as shown in Figure 1.1C. Hydrogel droplets are created at the tip of the inner capillary. Glass capillary devices have advantages of inherent wettability of glass surface, chemical resistant, and true 3D circular geometry. However, the typical fabrication method of the co-flow devices is to assemble glass capillaries manually, limiting the batch fabrication of devices. The quality of fabricated devices varies and depends on the person. Furthermore, co-flow glass capillary devices have a limitation of controlling the size of droplets [34].

Due to the difficulty of co-flow device fabrication, few studies has been carried out using co-flow capillary devices for droplet generation in tissue engineering application [42][43]. Sugiura *et al.* fabricated a micro nozzle array to control the size of alginate beads containing cells [42][43]. In [43], the device consisted of a nozzle for alginate pre-

polymer solution and air flow channel next to the nozzle. The alginate pre-polymer droplets were cut off by air flow, fell into $CaCl_2$ solution. Then, alginate droplets were crosslinked and created. The results showed that the encapsulated cells in the alginate droplets had a higher growth rate in comparison to alginate droplets generated by conventional methods because of high diffusion efficiency.

1.3.3 Flow-focusing Configuration

One of the most widely used microfluidic devices for droplet generation is flow-focusing devices. Although more technical effort is required for the fabrication of flow-focusing devices in comparison to T-junction, the flow-focusing devices offer better monodispersity and higher frequency of generating droplets up to around one thousand hertz [34]. In delicate experiments, such as cell encapsulation in microgels, flow-focusing devices are used more than other devices [34]. Also, flow-focusing devices offer a great flexibility in generating different size of droplets by adjusting the flow rate of both dispersed phase and continuous phase fluids [34].

Anna *et al*. first applied the flow-focusing geometry in a microfluidic two-phase flow [30]. In the device, dispersed phase and continuous phase fluids flowed into a cross-junction channel from different inlets, which results in generating either droplets or a jet stream. Several experimental studies have investigated the effect of different parameters on droplet generation regimes in flow-focusing devices which include the effect of the viscosity of the two phases [44][10] surface tension on droplet generation [30][45], the shape of the microfluidic channel [46][47], and the different methodologies in feeding the inflow [48].

In tissue engineering, flow-focusing devices are used to fabricate droplets of a biocompatible pre-polymer solution for encapsulating cells and drugs. Researchers have employed flow-focusing devices to generate droplets of several types of hydrogels

including magnetic hydrogel particles [49], phenyl boronic acid groups and poly(vinyl alcohol) [50], polyethylene glycol [51], gelatin methacrylate (GelMA) [52], and grapheme oxide GelMA [53]. For the tissue engineering application, the most important parameters are the size and type of hydrogel droplets which define the cellular microenvironment of the encapsulated cells [50]. Dang et.al fabricated flow-focusing devices with three different dimensions of microchannels and investigated the effect of device geometry and fluid flow rate on the generation of PEG hydrogel microparticles [51].

Over the last few decades, many studies have been conducted to investigate the cell encapsulation in microgels using flow-focusing microfluidic devices. A single cell was encapsulated into monodisperse picolitre drops using a flow-focusing device [54]. Kim *et al.* developed a new flow-focusing device that enhanced the cell viability by rapidly exchanging the oil phase [55]. When cell-laden alginate was cross-linked with calcified oleic acid, the toxic oleic acid was transformed into a harmless mineral oil and flushed out. A 3D flow-focusing device was introduced to generate the core-shell microcapsule for the efficient formation of cell spheroid by adding hillock in the flow-focusing device [56]. Wu *et al.* developed a microfluidic device integrated with fluorescence-activated sorting to increase the single cell encapsulation rate [57]. The device consisted of two modules−a flow-focusing module for the droplet generation and a cross-shaped hydrodynamic gating module for the droplet sorting. Capretto *et al.* demonstrated the formation and characterization of alginate/agarose microgels for the encapsulation of Sertoli cells [58]. The high cell viability and functionality of Sertoli cells encapsulated in alginate microgels demonstrated the effectiveness of this flow-focusing device for cell encapsulation. Köster *et al.* demonstrated to encapsulate, incubate, and manipulate individual cells in hydrogel droplets [59]. This study offered greater functionality of

microfluidic cell cytometers and cell sorters, allowing assay to be performed on individual cells in their own environment prior to sorting and analyzing. Masunaga *et al.* used the flow-focusing microfluidic device to encapsulate different kinds of cells in collagen microgels in the size range of 50-300 μm [60]. They cultured a variety of cells, including HepG2 cells, primary neurons, primary rat hepatocytes, NIH 3T3 mouse fibroblast cells, HUVECs, and MIN6 pancreatic cells in the collagen microgels. The results show that cells were attached to the surface of microgels in less than 2 hours. To study the proliferation of cells and the ability to create a 3D tissue construct, NIH 3T3-encapsulated microgels were placed in a PDMS mold to form a 3D tissue structure after 17 hours.

In addition, to experimental studies, theoretical and computational studies have been conducted to explain the dynamics of the flow-focusing process. Jensen *et al.* used Stokes flow theory to analyze numerically the formation of bubbles in the flow-focusing devices [61]. Lattice Boltzmann framework was also applied to understand the dynamics of flow-focusing devices [62]. In addition to physical model-based analysis, the adaptive meshing phase field model was also used to analyze the flow-focusing process [63]. Recently, researchers numerically investigated the effect of various parameters used for generating droplets, such as capillary number, viscosity, and geometry [64]–[66][67]. Theoretical and computational studies of the flow-focusing device are described in detail in Chapter 4. In this thesis, the flow-focusing devices were adopted to computationally and experimentally study the mechanism of hydrogel droplet generation.

1.4 Objectives of Thesis

Fabricating well-controlled hydrogel droplets are crucial in tissue engineering application. Microgel droplets could either use as cell culture platforms or as building blocks of tissue fabrication. Controlling the environment of encapsulated cells is important in order to

study cell-cell interaction and cell fate, as well as desired artificial tissue fabrication. A number of studies have been conducted to create biocompatible microgel droplets. These studies mostly focused on improving the biological and mechanical properties of hydrogel materials. However, due to the lack of systematic study of physics to generate hydrogel droplets in the flow-focusing devices, creating uniform droplets and controlling the size of hydrogel droplets remain challenging. Therefore, there is a critical need for a systematic study of the process to generate well-defined, cell-laden hydrogel droplet with controllable size. Although many studies have been conducted to investigate the effect of different parameters on water-in-oil droplet generation, these studies are not useful to apply in the hydrogel droplet generation because the fluid properties of hydrogels such as viscosity, density are much different from water. Therefore, the objectives of this thesis are

1. Develop microfabrication process of flow-focusing hydrogel droplet generation devices.
2. Theoretical and numerical study of droplet generation mechanism in a flow-focusing device.
3. Experimental study of droplet generation and cell-laden microgels fabrication.
4. Develop circular channel flow-focusing devices for the hydrogel droplet generation.

To achieve the objectives of this thesis, two different types of flow-focusing microfluidic devices were developed. Hydrogel materials with different viscosity and surface tension were used for continuous and dispersed phases to study the effect of different parameters on droplet generation. As an essential part of the project, a series of numerical simulations were carried out to study systematically the physics of droplet generation in the fabricated microfluidic devices. Finally, optimized parameters were applied to generate controlled hydrogel droplets with cells.

1.5 Thesis Structure

Chapter 1 describes a thorough literature review on tissue engineering, hydrogel materials used in tissue engineering application, and microfluidic platform used for droplet generation. Chapter 2 describes fabrication methods of flow-focusing microfluidic devices used for droplet generation. Basic microfabrication equipment and detail procedure of device fabrication are covered in this chapter. Chapter 3 describes the basic principal of droplet formation in two immiscible fluids. The effect of various parameters such as viscosity and density of the fluid, flow rates of fluids, and device geometry of droplet formation is presented. This chapter also includes the numerical simulation method to study the droplet generation mechanism of the flow-focusing device. The simulation results of droplet generation for the different regime are described. Chapter 4 presents the fabrication of hydrogel droplets in a flow-focusing device. This chapter illustrates materials of the dispersed phase and the continuous phase, the procedure to synthesize hydrogels, and experimental procedure to generate hydrogel microgels. Effect of fluid properties of dispersed and a continuous phase of the droplet generation is also discussed. Furthermore, the cell viability results of NIH 3T3 and MCF-7 cells encapsulated in hydrogel droplets are presented. Chapter 5 presents the introduction of a circular channel flow-focusing device and the fabrication procedure of the device. Also, the test results of the fabricated device are described in this chapter. Finally, Chapter 6 describes the contributions of this research along with suggestions for future works.

Chapter 2 Microfabrication of Microfluidic Flow-Focusing Devices

The microfluidic flow-focusing method has been well-established to generate droplets from two immiscible phases of fluids. This method has been widely used to fabricate droplets in a wide range of applications such as foods, cosmetics, drug delivery [68], and tissue engineering [69]. In this study, a flow-focusing microfluidic device has been developed to generate monodisperse hydrogel droplets. This chapter describes the development of a microfluidic flow-focusing device using the conventional microfabrication and softlithography techniques.

2.1 Overview of Microfluidic Device

The flow-focusing microfluidic channel fabricated consisted of two inlets, one junction, one chamber, and one outlet. The masks were designed using DraftSight software (Dassault Systèmes, Vélizy-Villacoublay, France) and printed on a transparent plastic film known as photo masks (CAD Art Services, Inc., CA, USA). After designing the microfluidic device, the microfluidic device was fabricated through replica molding method. Figure 2.1 shows the basic steps of replica molding method used in this work. Fabrication stems consist of mold fabrication, casting, replica removal, and bonding of replica to a substrate to provide a sealed device. The molds were fabricated via photolithography and mold casting was processed through the softlithography technique. To date, the most commonly used microfabrication technology in tissue engineering platforms is softlithography. The main advantages of softlithography include low cost, convenient fabrication steps, the easy control of deformation, structures in micro scale, and high compatibility with a broad range of biomaterials [70][71].

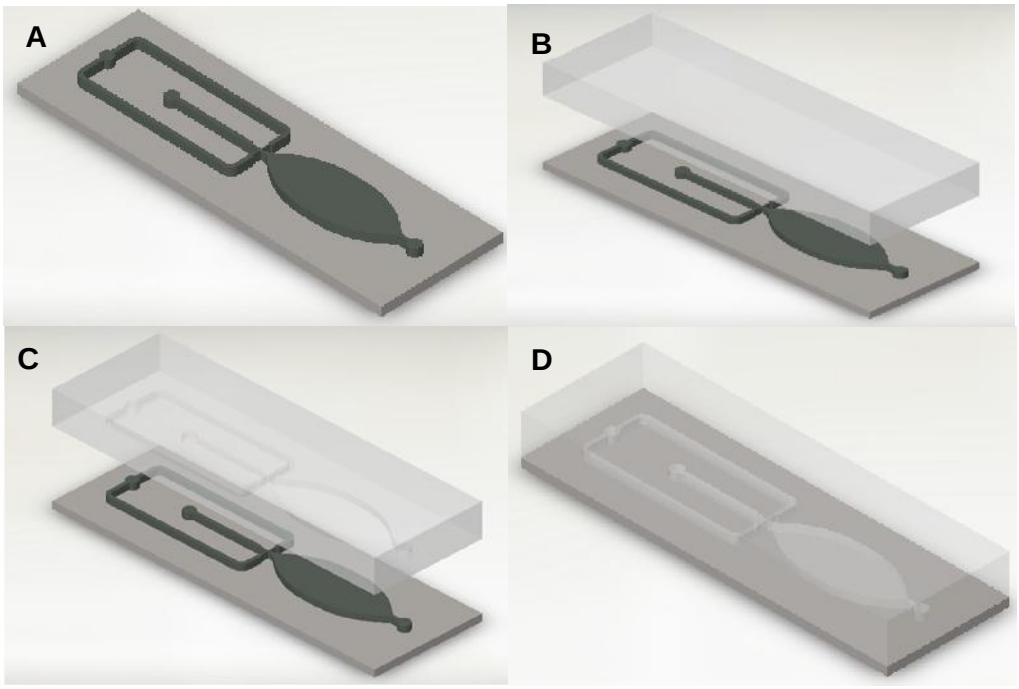

Figure 2.1 Microfabrication process. (A) Fabricating microchannel mold. (B) Casting PDMS on the fabricated mold. (C) Peeling off PDMS microchannel from the mold. (D) Bonding PDMS microchannel to a glass slide to build a device.

The most widely used biocompatible material used in softlithography is polydimethylsiloxane (PDMS). PDMS is gas permeable in which oxygen can be perfused inside the channel to supply enough oxygen to the cells inside the microfluidic device [72]. PDMS is transparent from 240 – 1100 nm wavelength. It means that PDMS is optically clear from long-wave UV to infrared radiation (IR) range, which allows several types of microscope systems to capture high-quality images. Also, PDMS is an electrical insulating elastomer with 750 kPa Young's Modulus, which makes it very suitable for generating the micro deformation dynamically. In addition, PDMS is non-toxic and biocompatible. Cells can be cultured and grown in the PDMS micro channels [72].

2.2 Mold Fabrication

Molds to form microfluidic channels were fabricated by a photolithography technique which is a well-established process for patterning microchannel structures out of a

photoresist on a substrate. Microfabrication process has been done in a class 100 (i.e. less than 100 particles in diameter of 0.5 µm or smaller per cubic foot) cleanroom facility at the school of engineering, UBCO. To fabricate a thick, thermally, and chemically stable microfluidic mold, the SU-8 2025 (Microchem, MA, USA) negative photoresist was used. SU-8 2025 is a viscous photoresist used to fabricate a thick layer of desired structure patterns. 20-80 µm thick photoresist coating can be achieved in a single spin coating of SU8-2025. Therefore, the photoresist was spin-coated twice to get 80-150 µm height microfluidic channels.

Figure 2.2 shows typical fabrication steps to create microfluidic channel molds. In the first step, a silicon wafer was washed with acetone and isopropanol three times and dried with air. Then, 1 ml of SU-8 was dispensed on the silicon substrate and spin-coated at 500 rpm for 10 seconds with an acceleration of 100 rpm/second, and then 1500 rpm for 30 seconds with the acceleration of 300 rpm/second (Table 2.1). Afterward, the photoresist on the wafer was baked at 65℃ for 5 min and then 95℃ for 10 min to remove the solvent. A photomask with desired microfluidic channel patterns was then positioned on top of the wafer. A glass fixed to a vertical shoulder was then placed on the photomask and pressed slightly to make contact between the photomask and wafer. The sample was exposed to a UV light at 365 nm and intensity of 11 mW/cm^2 for 40 seconds to create the required patterns on the photoresist. A post exposure bake took place directly after exposure for 10 min at 95 °C. Finally, the substrate was immersed in a SU-8 developer to remove unexposed areas of photoresist for 7 minutes. The thickness of SU-8 mold was measured using a micrometer. The baking times, exposure times, and developing times required for SU-8 are shown in Table 2.2. Following two sub-chapters describe details with regard to the spin coating, photomask alignment, and exposure.

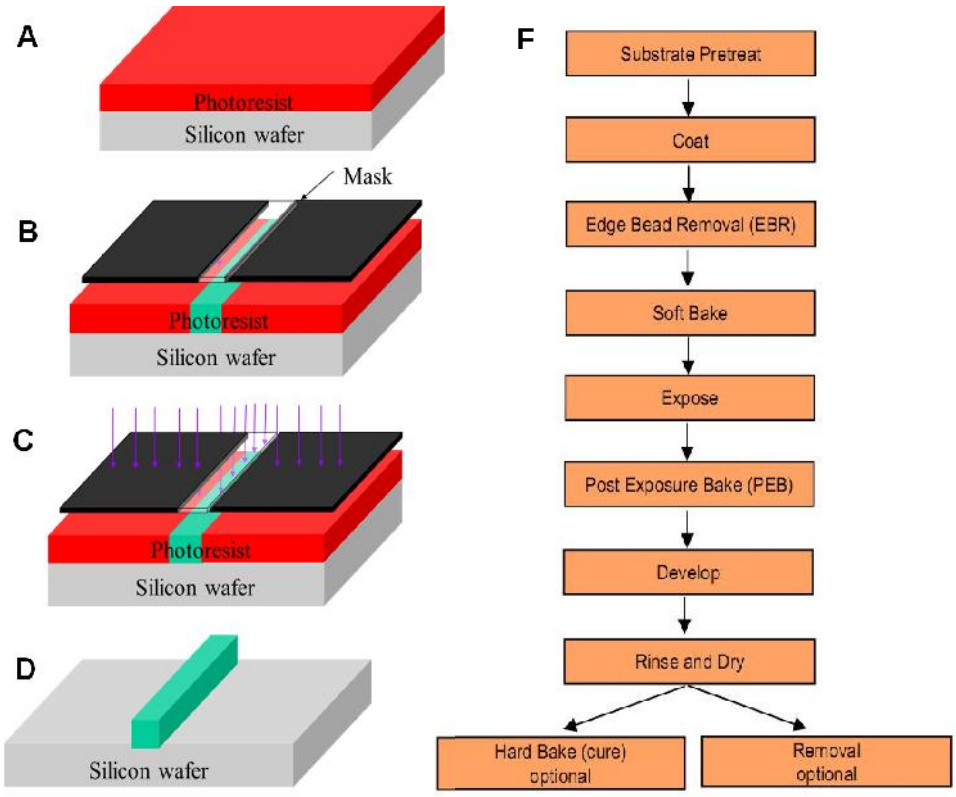

Figure 2.2 Photolithography process. (A) Photoresist coating. (B) Mask alignment. (C) UV exposing. (D) Developing. (F) Detail steps of photolithography process.

Table 2.1 Acceleration, RPM, duration, and cycles to coat SU8-2025 on a substrate

Parameters	Value Cycle 1	Value Cycle 2	Units
Acceleration	100	300	Rpm/s
Speed	500	1500	Rpm
Duration	10	30	Seconds
Cycle	2		

Table 2.2 Baking, UV light exposure, and developing time for fabricating different thickness of SU-8 coating on a substrate

Thickness	Soft Bake Times Minutes		Exposure Energy mJ/cm²	Post Exposure Times Minutes		Development Time Minutes
Micron	(65°C) Minutes	95°C Minutes		(65°C) Minutes	95°C Minutes	
45-80	0-3	6-9	150-215	1-2	6-7	5-7
85-110	5	10-20	150-215	2-5	8-10	7-10

2.2.1 Spin Coating

Spin coating process is widely used to coat a uniform layer of photoresist on a wafer. The process is to spin a wafer and spread a liquid photoresist by the acceleration of centrifugal force. Even though the thickness of the coating depends on the viscosity and concentration of materials, the thickness is ultimately controlled by the spin speed. A layer of SU-8 with a thickness of 25-80 μm could be created using a different spin coating speed and acceleration (Figure 2.3). Different baking processes and exposure times are correspondingly required to the desired thickness of the SU-8 layer (Table 2.2).

According to Figure 2.3, the higher spin coating speed creates, the thinner layer of photoresist. The maximum thickness of SU8-2025 that could be achieved is 80 μm at 1000 rpm speed. To get around 100 μm thickness of SU8-2025, the spin coating process was applied twice. SU8-2025 was spin coated on a Si wafer using a spin coating machine (Laurell Technologies Co., North Wales, PA, USA) in AMNF (Applied Micro and Nanosystems Facility) at UBCO. To spin the wafer with hi-speed RPM, the Si wafer is mounted on a chuck with suction pressure to firmly hold the wafer while spinning. The

spin coating machine is also equipped with a control panel to control various spin coating parameters.

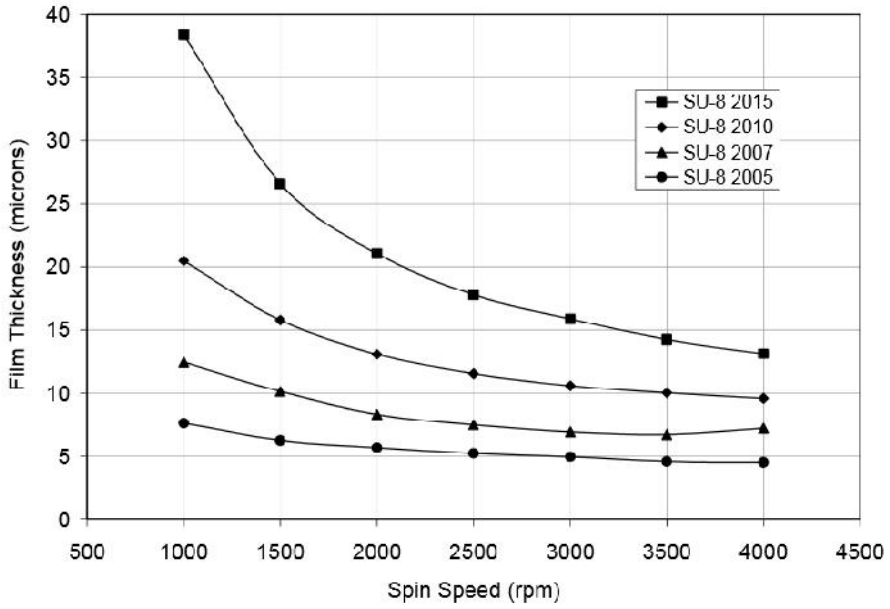

Figure 2.3 Thickness of coated SU-8 2000 versus thickness. (Adopted from [72])

2.2.2 Photomask Alignment and UV Exposure

A mask alignment system (Optical Associates Inc., San Jose, CA, USA) is used to transfer microchannel patterns from a photomask to the photoresist coated on the wafer. UV light attached to the mask alignment system illuminates the wafer to expose some parts of the photoresist onto UV light. The photomask is used to block some parts and prevent exposing the light pass through to the wafer. SU-8 is a negative photoresist which makes the exposed area cross-linked to create patterns while the unexposed area is washed away through a developing process.

The alignment system consists of a stage to hold the wafer, a stage to clasp the photomask, and a UV illumination system. The illumination system uses established a high-pressure mercury plasma arc discharge lamp. This lamp emits the ultraviolet (UV) light with the wavelength of 365 nm on to the photomask with uniform irradiance [73].

Better resolution can be achieved when the mask is in contact with the wafer. The duration of exposure depends on the types of photoresist and power of the UV lamp. For the microchannel mold fabrication in this research, the exposure time was 40 seconds.

2.3 PDMS Microchannel Casting and Bonding

One of softlithography techniques called a replica molding method was used to fabricate the microchannel on a silicone elastomer which is called PDMS [74]. The microfluidic chip was fabricated by pouring the 10:1 PDMS to curing agent mixture (SYLGARD 184, Dow Corning Co., Midland, MI, USA) over the molds in a petri dish. The petri dish was then placed in a vacuum desiccator for approximately 90 minutes or until all the bubbles are disappeared. The mold was then placed in an oven at 70 °C for three hours to cure PDMS. Finally, the PDMS with the engraved microfluidic channel was peeled off from the mold as shown in Figure 2.1C. Tubing holes for the inlet and outlets of the PDMS were punched using a biopsy punch. The PDMS channel was then bonded to the glass slide. To get a perfect sealing and permanent bonding between the PDMS and a glass slide, the surfaces both PDMS and the glass slide were cleaned and dried and then a handheld corona discharge plasma treatment machine (Electro-Technic Products, Chicago, IL, USA) was used to treat oxygen both surfaces for 5 minutes [75]. Since the corona discharger activated the surfaces to create free oxygen, the PDMS and glass being in contact together form a strong co-valent bonding as shown in Figure 2.4. However, this causes the bonding free channel area that is turned to hydrophilic due to the plasma treatment. Since a hydrophobic channel is needed to create hydrogel droplets in oil [76], a post-bake process is required to change the surface property of the microchannel. To do that, the microfluidic device was placed in an oven at 70^{o}C for 5 hours for the hydroxyl (-OH) group on the channel to be eliminated to create a hydrophobic microfluidic channel. Figure 2.5 shows the fabricated flow-focusing device. The sealing of the device was

checked with the injection of a colored liquid as shown in Figure 2.5A. The detail view of cross-junction of the flow-focusing device is shown in Figure 2.5B.

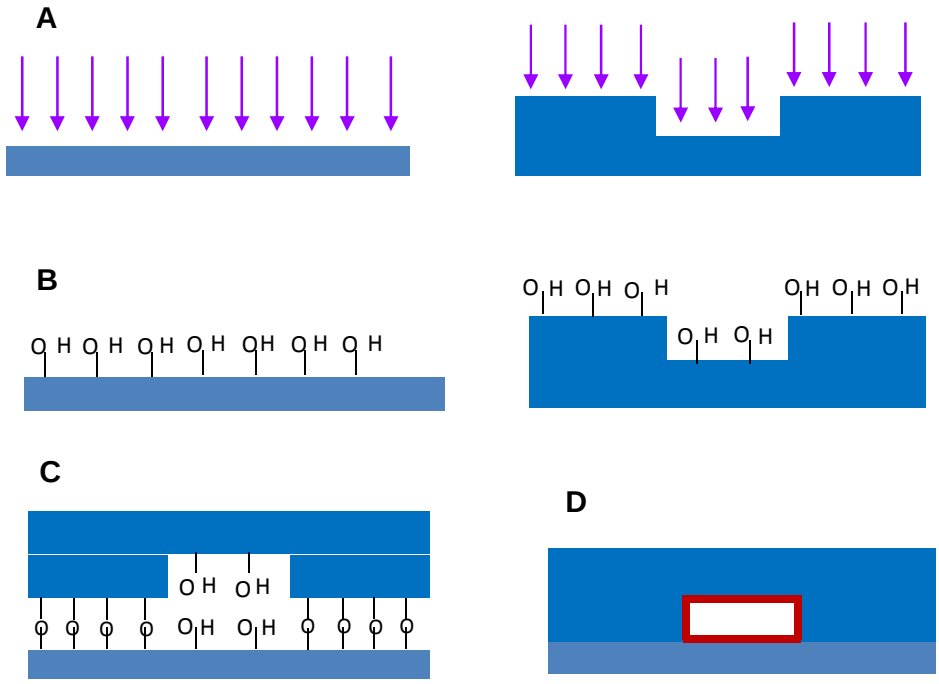

Figure 2.4 Oxygen plasma treatment and bonding mechanism. (A) Activation of the surfaces of PDMS and glass slide with the oxygen plasma. (B) Oxygen activated surface with hydroxyl (-OH) group. (C) Co-valent bonding of between the PDMS and glass slide. (D) Permanently bonded and sealed device (Red color shows hydrophilic surface for requiring further baking time).

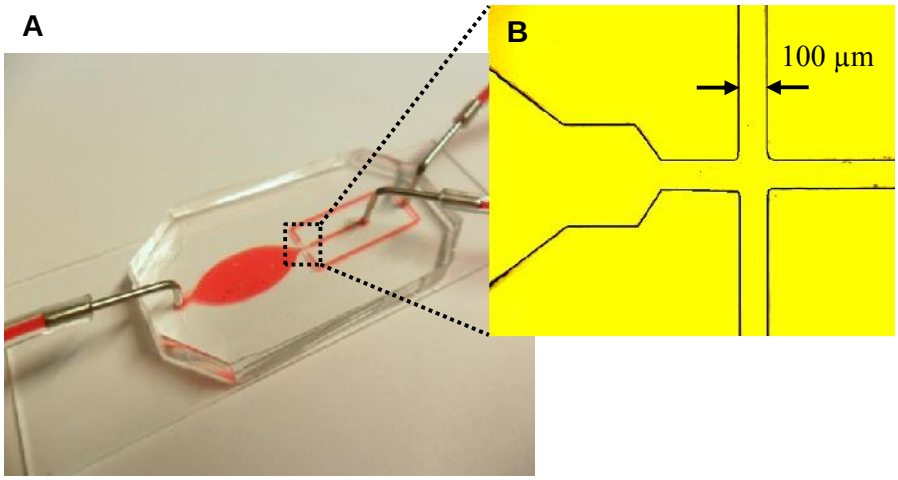

Figure 2.5 Fabricated device. (A) Photographic image of testing fabricated flow-focusing device field with red colored liquid. (B) Microscopic image of flow-focusing cross- junction channel.

2.4 Summary

In this chapter, the fabrication of the flow-focusing device using the replica molding technique was described. The PDMS microchannel was fabricated by casting PDMS on the microfabricated mold. The cured PDMS microchannel was peeled off from the mold and bonded to a glass slide to complete the flow-focusing device. To make a irreversible bond between the PDMS and the glass slide, a handheld corona discharge plasma treatment machine was used to treat oxygen plasma on both surfaces of the PDMS and glass. The leakage and blockage of the device were tested by injecting a colored liquid into the channel, and no leakage was observed. The developed flow-focusing device was used to fabricate hydrogel droplet generation for tissue engineering application.

Chapter 3 Theoretical and Computational Study of Droplet Generation

In this chapter, theoretical backgrounds behind the droplet formation mechanism in microfluidic flow-focusing devices as well as the effect of different parameters on droplet sizes are described. To verify the theoretical mechanism of droplet generation, a computational study using a finite element analysis (FEA) software was carried out. Computational study results were used to investigate parameters for hydrogel droplet generation experiments.

3.1 Theoretical Backgrounds

When a liquid is injected into another immiscible fluid in a microfluidic device, the liquid ultimately breaks into droplets through either dripping or jetting mechanism. At a slow flow rate, the liquid drips at the orifice channel which is called a dripping regime, whereas, at a higher flow rate of flows, the liquid makes a thin stream that breaks into droplets away from the orifice channel and this regime is called a jetting regime. The formation of water droplets at a faucet is a good example to understand how these regimes are created in the microfluidic devices. At a slow flow rate, water droplets are created close to the faucet (Figure 3.1A). In this case, surface tension causes water to form droplets at the tap, and the droplets are detached when the gravitational force overcomes an interfacial tension force. At a higher flow rate (Figure 3.1C), the jetting regime occurs because the inertia force dominates the interface tension. At the downstream, the jet stream breaks into droplets away from the tap because of Rayleigh-Plateau instability. Due to this theory, the jet stream of fluids was always unstable and eventually forms droplets to minimize the surface energy [31]. Any perturbation in the jet stream leads in a slightly thinner jetting. The Laplace pressure (the pressure difference

between the inside and the outside of a curved surface) within the thinner region of the jet stream increases because of the curvature of the interface.

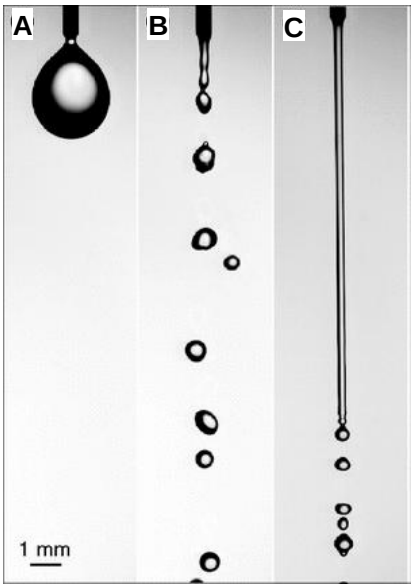

Figure 3.1 Droplet formation of water from a faucet. (A) Formation of droplets at a low flow rate. (B) Formation of droplets slightly increasing by the flow rate. (C) Formation of a jet stream of water at a high flow rate (Adopted from [117]**).**

This higher pressure pushes the fluid within the jet stream to the sides, and makes the thin region become thinner. Finally, the droplets break up once the gravitational force overcomes the interfacial tension force. However, in the case of the microfluidic device, the droplet formation occurs due to the balance between the surface tension force and the viscous drag force of the outer liquid [77]. When a liquid is injected into another immiscible liquid in a microfluidic device, the mechanism of droplet formation is changed because of the presence of the surrounding viscous liquid [31].

There are various microfluidic device geometries for the droplet generation. Among them, T-junction, flow-focusing, and co-flow geometries are most common in droplet generation (Figure 1.1). A flow-focusing microfluidic device has a well-established geometry due to the advantage of fabricating high throughput monodisperse droplets. As shown in Figure 1.1 B, in the flow-focusing device, there is an intersection of two

channels to form a cross junction. A dispersed phase fluid flows into a central channel and continuous phase fluid flows through side channels to surround the dispersed phase fluid at the junction. Then, either a jet stream or droplets of the dispersed phase fluid are created. The formation of either droplets or jet stream depends on different parameters, such as the geometry of devices [78][79], fluid flow rates, viscosity, density, and interfacial energy between two fluids [80][81][10]. These parameters can be summarized into two non-dimensional numbers, which are called “capillary number” and “Webber number”. These two numbers govern the formation of droplets or jet stream in flow-focusing devices. The capillary number describes the relationship between the viscous force and interfacial force [82] as follows,

$$Ca = \frac{\mu U}{\sigma} \tag{2.1}$$

, where μ and U represent the viscosity and velocity of fluids, respectively, and σ represents the interfacial tension between the two immiscible fluids. The webber number describes the relationship between the inertia force and the interfacial force [82] as follows,

$$We = \frac{\rho U^2 D}{\sigma} \tag{2.2}$$

, where ρ, U, and D represent the density, velocity of dispersed phase fluid, and the channel hydraulic diameter, respectively, and σ represents the interfacial tension between the two immiscible fluids [83]. These nondimensional numbers are important to predict the formation of droplets and jet stream and design experimental conditions.

To better understand the droplet generation mechanism in the flow-focusing device, three regimes of droplet formation (i.e., squeezing, dripping, and jetting regime) are described in this chapter. The models developed to investigate the relationship between fluid properties and droplet sizes are also presented. Figure 3.2 shows three droplet generation modes in the flow-focusing device. In two-phase microfluidic systems, dispersed and continuous phase fluids basically are injected into the device from two separate microchannels. Typically, fluids meet at the junction and then the continuous phase surrounds the dispersed phase and the two-fluid interface deforms. At this point, if the free surface instabilities between the phases are large, droplets develop and finally break up from the dispersed phase. In contrast, a jet stream is formed if the free surface instabilities are minimized. These instabilities come from the competition between stabilizing and destabilizing forces at the interface between two phases. Shear force and fluid inertia are examples of forces that promote the formation of jet stream while other forces like capillary pressure and interfacial force promote the destabilization and creating droplets. Three regimes of droplet formation are described in detail following subchapters.

3.1.1 Mode 1- Squeezing

As shown in Figure 3.2A (Mode 1), at the very low capillary numbers of continuous and dispersed phase, the dispersed phase entering into the orifice channel blocks the channel. This results in an increase of the upstream hydrostatic pressure on the continuous phase channel. In order to sustain the constant flow rate, the syringe pump increases the pressure applied to the continuous phase fluid streams. This leads to creating a neck of the dispersed phase at the entrance of orifice channel. Finally, the narrowing neck becomes unstable and breaks to form a droplet of the dispersed phase fluid [84]. Droplets

are formed by the equilibrium of the interface tension and hydrostatic pressure field. Gastecki *et al.* introduced a rate-of-flow-controlled breakup model in the flow-focusing device at a low flow rate [84][85][82]. The rate-of-flow-controlled break up model describes that the size of the droplets is only related to the ratio of flow rates of the dispersed phase and continuous phase fluids in case of a low flow rate.

3.1.2 Mode 2- Dripping

For the dripping regime, the combination of capillary instabilities and viscous drag defines the droplet formation in a flow-focusing device. A study demonstrated that either capillary instability or viscous drag alone could not induce the droplet formation [82]. As shown in Figure 3.2B (Mode 2), by slightly increasing the flow rate of fluids, the dispersed phase becomes unstable because the surface tension force seeks to minimize the interfacial area by creating a spherical droplet, while the viscous force of the continuous phase tries to suppress the formation of the droplet. When the shear force of the continuous phase fluid overcomes the interfacial surface tension, that keeps droplets attached to the aqueous neck, the droplet breaks up [83]. Dripping regime investigated based on shearing model. The shearing model emphasizes that the diameter of droplets is inversely related to the capillary number [10].

3.1.3 Mode 3-Jetting

The jetting regime occurs either when the Webber number (We) of the dispersed phase fluid is high or the capillary number of the continuous phase is high. On the one hand, when the Webber number of the dispersed phase is greater than 1 due to either high dispersed phase flow rate or high density, the inertia force dominates interfacial tension forces. This moves the aqueous neck downstream to generate the long, unstable jet stream of the disperse phase fluid. On the other hand, when the capillary number of the

continuous phase fluid is high due to either large continuous phase flow rate or high viscosity, the viscous drag force of the outer continuous phase fluid pulls the dispersed phase fluid enough to overcome the interfacial tension force. This also results in a long thin stream of the dispersed phase fluid. In other words, if the viscous force of the continuous phase becomes more significant in comparison with the interfacial surface energy, or if the inertial force of the dispersed phase dominates the interfacial energy, the perturbation is suppressed and results in a jetting regime [82]. This jet stream is unstable due to instabilities and eventually breaks into droplets at the downstream of the channel. Based on Rayleigh- Plateau instability, the dispersed phase fluid becomes unstable at the downstream of the channel because the surface tension of the dispersed phase tries to minimize the interfacial area by creating a spherical droplet. Though the viscous force of the dispersed phase tries to suppress droplet formation, the higher viscous force of the continuous phase than that of the dispersed phase finally overcomes the interfacial tension to form droplets (Figure 3.2C).

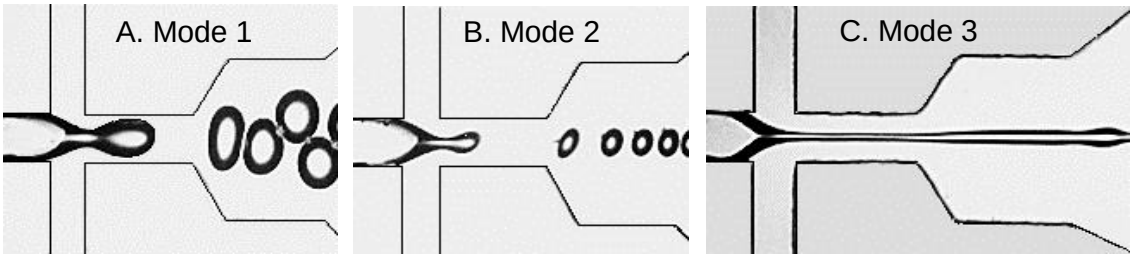

Figure 3.2 Droplet formation mechanisms in the flow-focusing device. (A) Mode 1- squeezing regime at very low flow rate and very low capillary numbers of fluids. (B) Mode 2-dripping regime at higher flow rate and moderate capillary numbers of fluids. (C) Mode 3-jetting regime at high capillary number of fluids.

Figure 3.3 shows the phase diagram of the dispersed phase and continuous phase in a flow-focusing device [86]. The figure shows the capillary numbers of dispersed phase versus continuous phase. At the low capillary numbers, droplets are easily created in the

flow-focusing device. However, a jet stream is created due to the increment of capillary numbers by increasing either flow rate or viscosity of fluids. The transition of dripping to jetting regime occurs at the capillary number around 1.

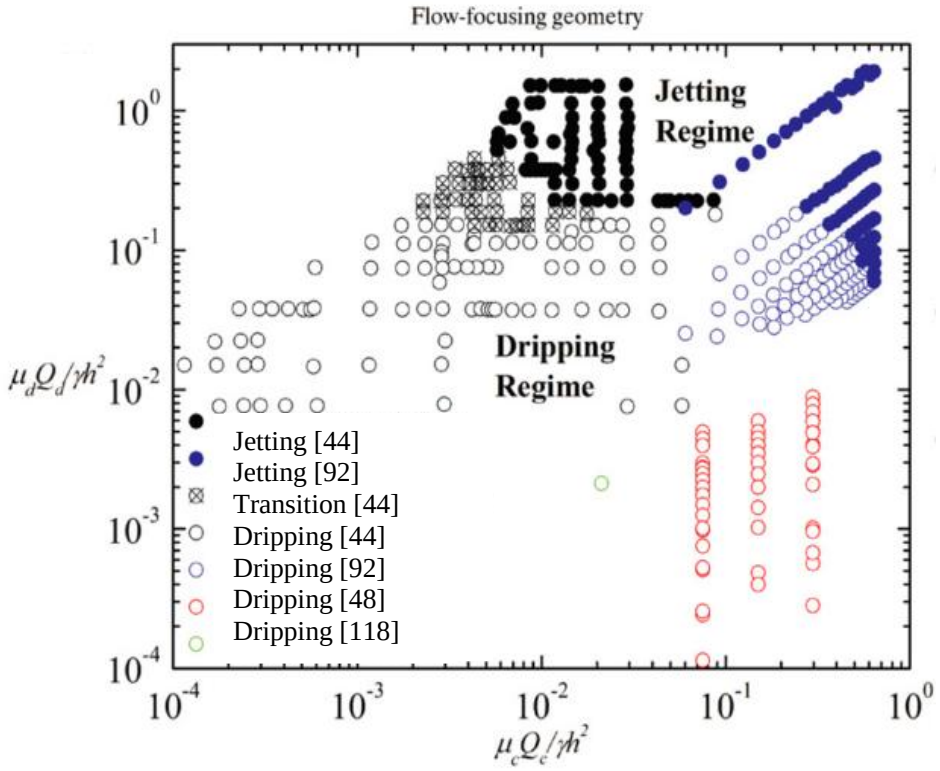

Figure 3.3 Phase diagram and formation of dripping and jetting regime in a flow-focusing device (Adopted from [86]**).**

The fundamental equations of mass, momentum and energy conservation are used to investigate the droplet formation in a microfluidic device. Since the theoretical study of droplet generation requires many parameters, most of droplet generation mechanisms are analyzed using a numerical method to investigate shear forces and pressure changes in the microfluidic devices using separated solution domains (e.g., dispersed phase and continuous phase). Another important factor in the numerical simulation of droplet generation is to resolve the phase interface since parameters, such as density, viscosity and pressure, are not continuous between two phases.

Moreover, most of previous studies have investigated the droplet formation and breakup of aqueous solutions in oil. However, the fluid dynamics of the biocompatible pre-polymer solution is different from water, which makes optimized water-oil parameters less useful in manipulating hydrogel droplet generation. Viscosity and surface tension are among the most important parameters influencing droplet generation regime. With the emergence of new biomaterials and hydrogels, the range of viscosity and surface tension values in microfluidic flow-focusing devices have been extended. Therefore, it is important to characterize the droplet formation and breakup regimes in microfluidic flow focusing systems for a wider range of viscosity, surface tension and capillary numbers which have not been studied for hydrogel pre-polymer solutions. Thus, this research utilized a numerical simulation software, COMSOL Multiphysics, to optimize the flow rate, droplet sizes, and droplet generation mechanism with various viscosities, surface tension, and capillary numbers for hydrogel pre-polymer solutions in oil using the flow-focusing device geometry.

3.2 Computational Simulation

Computational simulation software (COMSOL Multiphysics 4.3b, Comsol Inc., Burlington, MA, USA) was used to simulate the hydrogel droplet formation in a flow-focusing device. The simulations were carried out in the 3D domain to study the physics of three different regimes in two-phase flow microchannel (dripping, squeezing, and jetting) and also study in detail how to create uniform hydrogel droplets in a microchannel flow-focusing device.

3.2.1 3D Modeling of Device Geometry

Figure 3.4 shows the dimension of the flow-focusing device with the rectangular cross sectioned microchannel. The modeling was carried out using only a rectangular cross-section because of observations of devices. The geometry of flow-focusing devices was

defined in the global definition section of COMSOL. The simulations were carried out in 3D to consider the effect of all constraints realistically. To build the 3D model of the flow-focusing device, each cross-section of inlets was created in different work planes and then extruded. A square of 90×90 μm^2 was created in a *XY* plane and then extruded in the distance of 300 µm. Another square of 90×90 μm^2 was created in a *ZY* plane and then extruded in the distance of 600 µm. Figure 3.4 also shows the modeling domain. While Fluid 1 to be dispersed into hydrogel droplets enters into the central inlet, Fluid 2 (continuous phased oil) enters into both sides inlets and flow through the main channel.

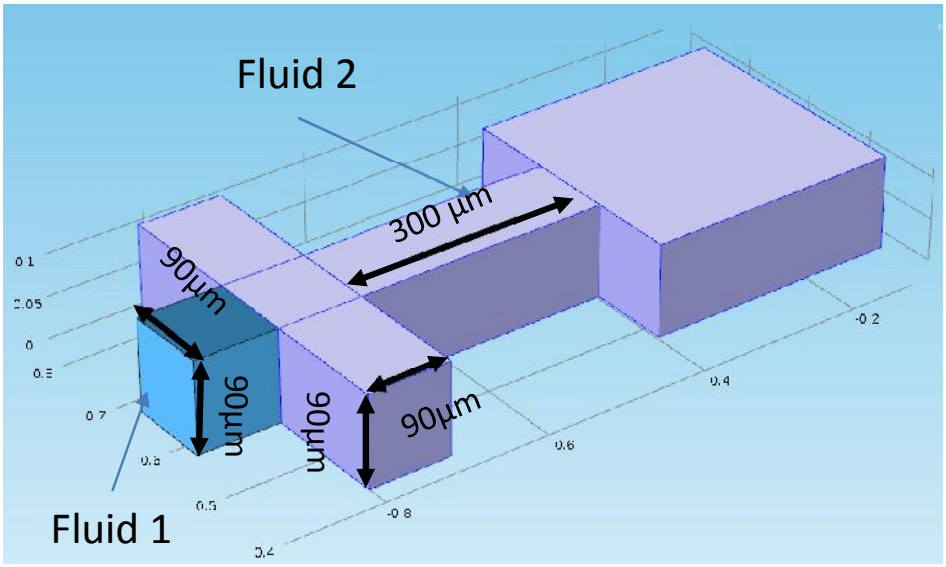

Figure 3.4 Geometry and fluids domains of the flow-focusing device simulation

3.2.2 Numerical Model of Two Phase Flow

In this study, "Laminar Two-Phase Flow, Level Set" interface in COMSOL Multiphysics 3.3b (Comsol Inc., Burlington, MA, USA) is adapted to simulate the hydrogel droplet generation. The laminar flow was chosen because the Reynolds number (Re =$\frac{\rho V D}{\mu}$) for all the cases were less than 4. The fluids were assumed as Newtonian and incompressible fluids. The level set methods, a class of numerical techniques, were first introduced by

Osher and Sethian and deal with fluid-interface motion that is represented implicitly. The equation of the fluid-interface motion is numerically approximated. Level set methods are particularly useful for problems in which the topology of the evolving interface changes during the course of events. The fluid interface between the dispersed phase and continuous phase is set up by a momentum transport equation, a continuity equation, and a level-set equation [87]. These equations are as follows:

$$\frac{\partial \mathbf{u}}{\partial t} + \rho(\mathbf{u}.\nabla)\mathbf{u} = \nabla.[-p\mathbf{I} + \mu(\nabla\mathbf{u} + (\nabla\boldsymbol{u})^T)] + \mathbf{F}_{st} \tag{2.3}$$

$$\nabla.\boldsymbol{u} = 0 \tag{2.4}$$

$$\frac{\partial \phi}{\partial t} + \boldsymbol{u}.\nabla\phi = \gamma\nabla.\left(-\phi(1-\phi)\frac{\nabla\phi}{|\nabla\phi|}\right) + \varepsilon\nabla\phi) \tag{2.5}$$

, where ρ is density (kg/ m^3), u velocity (m/s), t time, μ dynamic viscosity (Pa·s), *p* pressure (Pa), and F_{st} surface tension force (N/m^3). ϕ is the level set function which is in the range of 0 to 1. The value of ϕ at the interface is considered to be 0.5 and ϕ values less than 0.5 corresponds to Fluid 1, whereas ϕ values greater than 0.5 corresponds to Fluid 2. γ and ε are the numerical stabilization parameters. ε determines the thickness of the interface and it should have the same order as the computational mesh size of elements where the interface propagates. γ determines the amount of re-initialization of the level set function. A suitable value for γ is the maximum value for the velocity field of u. 1 m/s was used for the re-initialization parameter (γ) which is an approximate value of

maximum speed occurring in a fluid flow. The density and viscosity are calculated as follows,

$$\rho = \rho_1 + (\rho_2 - \rho_1)\square \quad (2.6)$$

$$\mu = \mu_1 + (\mu_2 - \mu_1)\square \quad (2.7)$$

, where ρ_1, $\rho_{1,}$ $\mu_{1,}$ and μ_1 are densities and viscosities of Fluid 1 and Fluid 2.

3.2.3 Fluid Properties for Simulation

Fluid 1 entering into a center inlet is specified for hydrogel pre-polymer solution. Fluid 2 entering into side inlets and flows through the main channel is specified for oil with a surfactant. Properties of Fluid 1 and 2 that used in the computational simulation, such as densities, dynamic viscosities, and surface tension, are listed in Table 3.1. These values obtained from the experimental measurement. The viscosity was measured using a Viscometer (Cannon Instrument Company, State College, PA, USA). Various properties of fluids were used to study the effect of parameters (density, viscosity, surfactant, and flow rates) on hydrogel droplet generation mechanisms and droplet size.

3.2.4 Boundary Conditions and Initial Condition

Boundary conditions of the inlet and outlet were set to describe fluid flow conditions at the inlets and outlet. Normal inflow velocity was defined for the inlet nodes (inlet and outlets are shown in Figure 3.5) of the simulation model. Pressure without viscous stress (p_0) was chosen for the outlet boundary condition.

Table 3.1 Material properties used in computational simulation. (Values of interfacial tension adopted from [119] [120] **and they measured surface tensions by the pendt drop method using a Rame-Hart model number 500-F1 advanced goniometer).**

	Density (kg/m^3)	Viscosity (mPa·s)	Interfacial tension between oil and GelMA at 20 °C (mJ/m^2)
GelMA 5% wt	1300	2.8	
GelMA 8% wt	1500	4.9	
Mineral oil	870	27	48
Mineral oil+ 3% surfactant	890	30	5
Mineral oil+ 20% surfactant	1120	57.7	5
Hexadecane	780	3.3	46
Hexadecane + 3% surfactant	1020	4.2	5
Hexadecane + 20% surfactant	1080	6.7	5

Figure 3.5 shows the boundary condition for the simulation. The wetted wall boundary condition applies to all solid boundaries with the contact angle of pi/4 and slip length equal to the mesh size parameters h. In wetted wall boundary condition, the fluid-fluid interface can move along the wall, and this boundary condition is proper for walls in contact with the fluid-fluid interface. The contact angle is the angle between the fluid interface and the solid wall at points where the fluid interface attached to the wall. The slip length is the distance to the position outside the wall where the extrapolated tangential velocity component is zero (Figure 3.6).

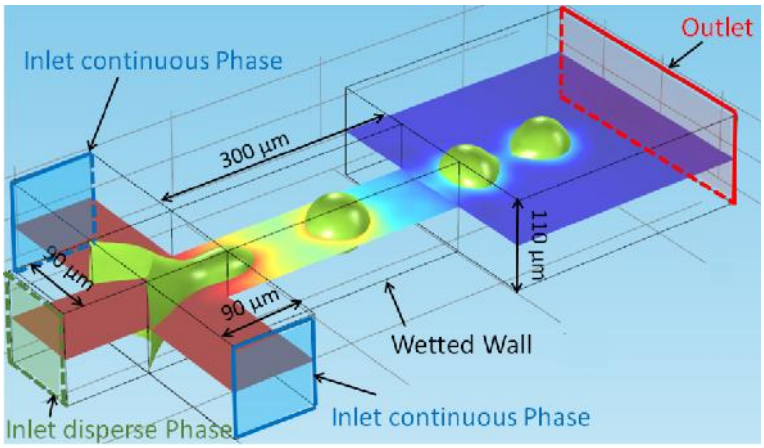

Figure 3.5 A detail schematic of computational domain used for numerical simulation and boundary condition of the flow-focusing device.

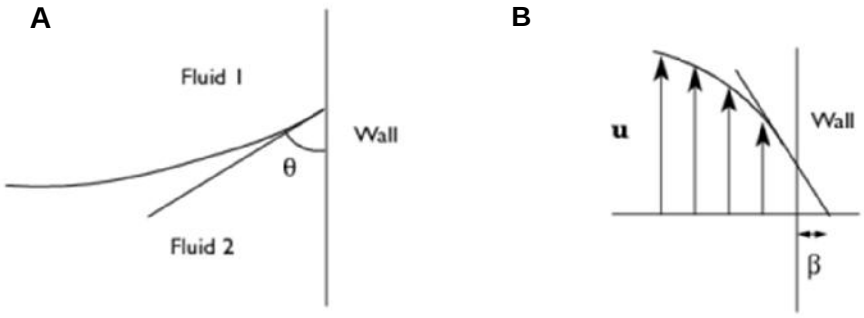

Figure 3.6 Illustrations of contact angle and slip length. (A) θ is the contact angle at interface/wall contact points and (B) β is the slip length.

Figure 3.7 shows the computational mesh grid used in the simulation. A numerical mesh grid was adopted after performing grid dependence studies with different grid resolutions.

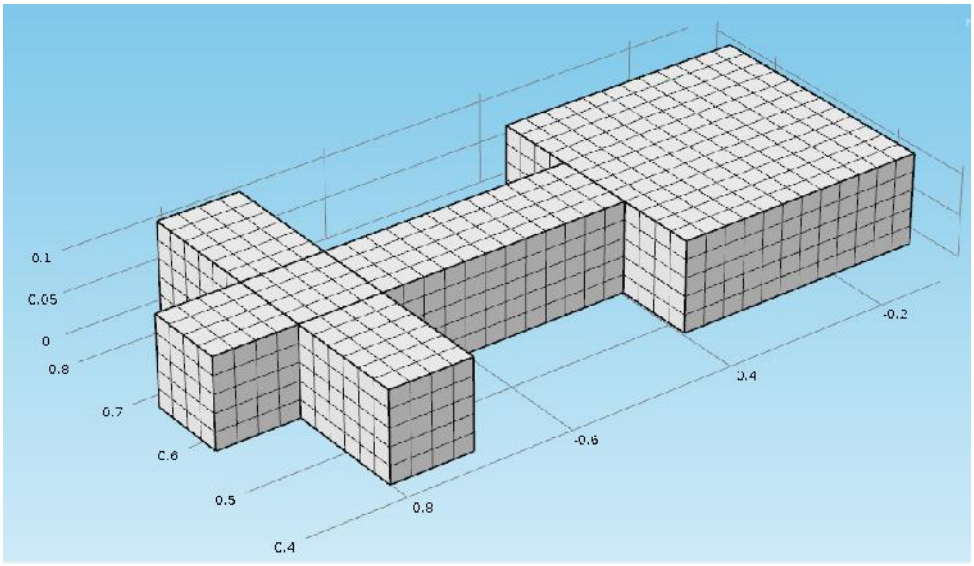

Figure 3.7 A 3D model of the computational mesh grid.

3.3 Computation Simulation Results and Discussion

3D Computational simulations were conducted with the same geometry of the fabricated flow-focusing devices and same fluid properties of the gelatin methacrylate (GelMA) hydrogel droplet generation experiments which will be discussed in Chapter 4. Figure 3.8A shows the simulation results of the change in the droplet size of 5 wt% GelMA versus the various flow rates of oil with 3wt% surfactant and Figure 3.8B shows the results of 8wt% GelMA. The droplet size was decreased by increasing the flow rate of the continuous phase. The droplet size of 8 wt% GelMA, which was highly viscous, was not decreased anymore at a flow rate greater than 30 μL/min (Figure 3.8B). The minimum size of 8 wt% GelMA could be achieved around 40 μm when the flow rate of the dispersed phase was 2 μL/min.

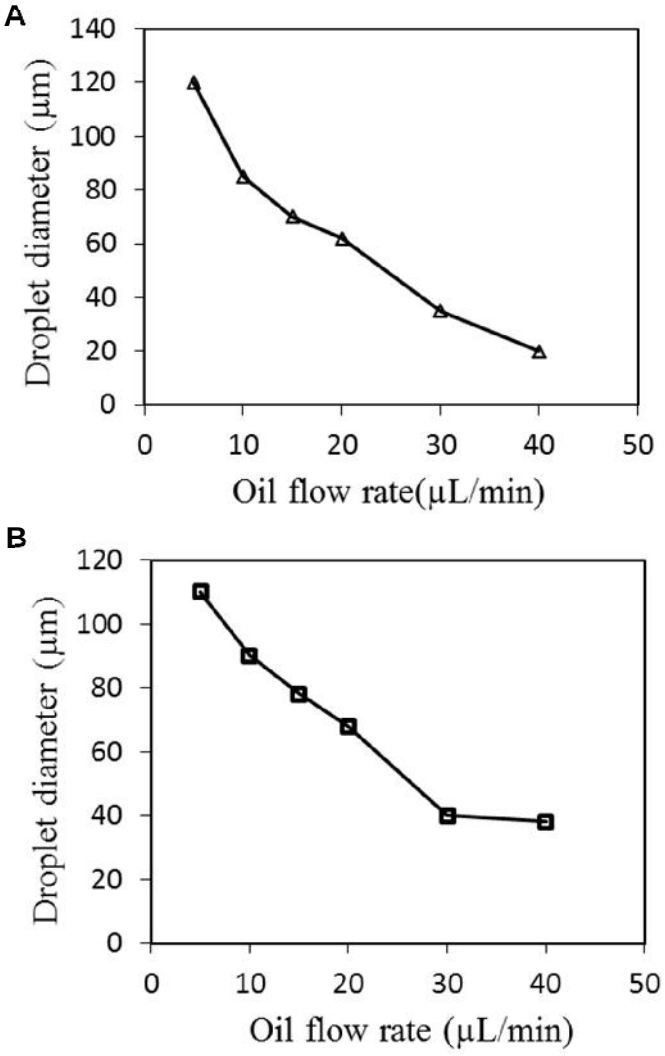

Figure 3.8 Simulation results of the change in the GelMA droplet size. (A) Diameter of GelMA droplets (5 wt%) under the various flow rates of continuous fluid, mineral oil with 3 wt% surfactant (Span 80). (B) Diameter of GelMA microgels (8 wt%) under the various flow rate of continuous fluid, mineral oil with 3 wt% surfactant (Span 80). Flow rate of disperse phase (GelMA) was

Figure 3.9A shows the computational simulation result of the squeezing regime. The simulation was conducted to visualize the physics of droplet generation during squeezing regime. The flow rate of the dispersed phase (Qd) and the continuous phase (Qc) was 2 μL/min and 5 μL/min, respectively. Fluid properties of 5 wt% GelMA were used for the

dispersed phase and oil with 3 wt% surfactant (Span 80) was used for the continuous phase.

Two different regimes (i.e., squeezing and dripping) was numerically simulated in the flow-focusing geometry. In the squeezing regime, droplets were generated in the orifice channel (Figure 3.9A). As discussed in Chapter 3.1.1, this regime occurred when the flow rate and viscosity of fluids were low. In this regime, the dispersed phase flow (GelMA) enters into the orifice and block the channel, resulting in an increase of the upstream hydrostatic pressure (pressure at point 1 in Figure 3.9A) in order to sustain the constant flow rate. The diameter of the droplet, in this case, was greater than the diameter of the orifice channel. The pressure changes in the microfluidic channels are shown in color. It was found that during the squeezing regime when the dispersed phase blocked the channel, the pressure at point 1 built up to 2 kPa. When the dispersed phase blocks the channel in the squeezing regime the difference between before (point 1in Figure 3.9A) and after (point 2 in Figure 3.9A) cross-junction pressure was around 0.8 kPa. Thus, the droplets break up in the squeezing regime because of the pressure build-up at the cross-junction. Garstecki *et al.* investigated the mechanism governing the squeezing regime in a flow-focusing device when the disperse phase is a gas [84]. Gas droplets were generated in a flow-focusing device at low flow rates, which matches well with the results of generating hydrogel droplets at low flow rates. Both studies demonstrated that droplets can be generated at low flow rates under the squeezing regime.

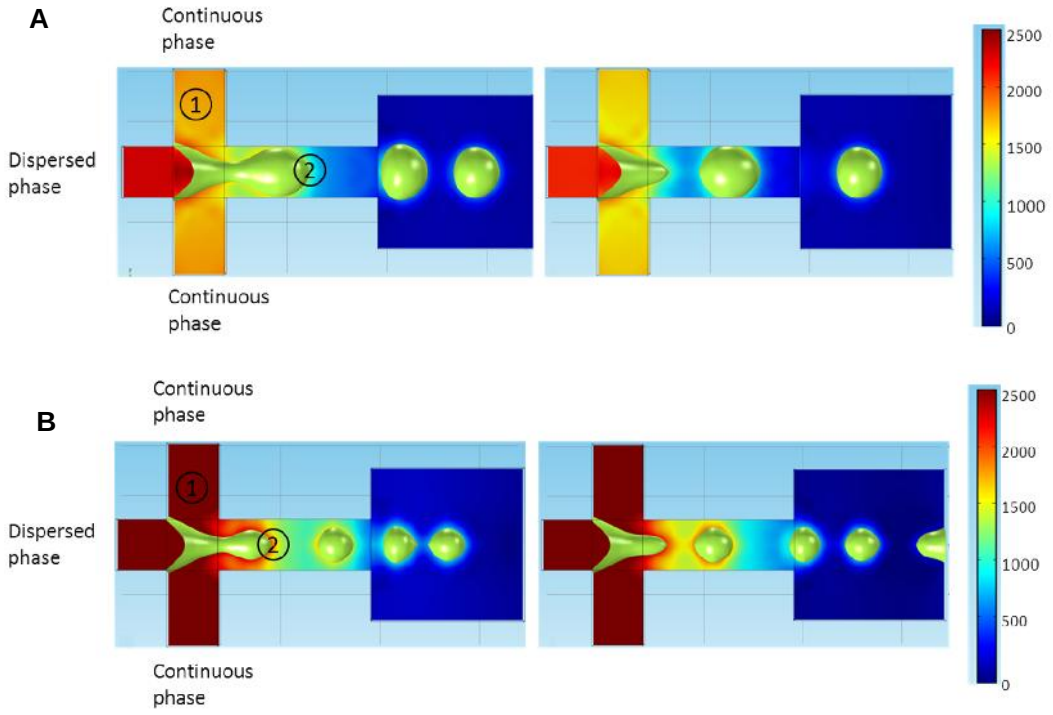

Figure 3.9 Computational simulation results of droplet generation during (A) the squeezing regime and (B) dripping regime.

During the dripping regime (shown in Figure 3.9B), the flow rate or viscosity of the continuous phase was much greater than the dispersed phase. As discussed in Chapter 3.1.2, droplets broke because of Rayleigh-Plateau instability. In fact, the dispersed phase fluids tended to minimize its surface tension energy by forming a spherical shape. Therefore, the neck was formed by the continuous phase fluid, which dragged the dispersed phase fluid to the orifice channel. When the viscosity of the continuous phase fluid overcame the interfacial force of the disperse phase, the droplets were cut off. The droplets were smaller than the width of the orifice channel. In the dripping regime, the pressure does not change much before or after droplet generation. The pressure difference between before (point 1 in Figure 3.9B) and after (point 2 in Figure 3.9B) cross-junction is around 0.4 kPa, which is smaller than the squeezing regime (0.8 kPa). Therefore, the droplets break up due to the Rayleigh-Plateau instability theory.

3.4 Summary

Theoretical background of droplet generation was discussed in this chapter. Three different regimes of droplet formation in a flow-focusing device: squeezing, dripping, and jetting regime was described. Either droplets formation or jet stream depends on different parameters, such as the geometry of devices, fluid flow rates, viscosity, density, and interfacial energy between two fluids. To study the effect of all these parameters non-dimensional capillary numbers, which are called “capillary number” and “Webber number” introduced in this chapter. At a high capillary number of dispersed and continuous phases, a stream of the jet is created in a flow-focusing device. However, at the capillary number below 1 the droplets are created in a flow-focusing device. To study the mechanism of droplet formation in different regimes, a computational study using COMSOL software was carried out. Computational simulation results were used to optimize parameters for experiments. The geometry of simulation, boundary condition, fluid properties, mesh grids, and simulation results was described in this chapter. The simulation results were comparable to the previous studies and matched well with the experimental results of this study. Simulation results show that the droplets are formed in the squeezing regime because of the pressure gradient in the continuous phase channels while the formation of droplets in a jetting regime is because of the viscous force of the continuous phase.

Chapter 4 Experimental Study of Hydrogel Droplet Generation and Cell Encapsulation

In this chapter, the experimental study of the GelMA droplet generation in the flow-focusing device is described. To achieve a wider range of capillary numbers, this study quantitatively investigated the GelMA droplet generation mechanism in the flow-focusing device from experiments. The effects of several key parameters, such as the concentration of hydrogel, the concentration of surfactant, and the viscosity of continuous and dispersed phases were experimentally studied. All experimental data were summarized by capillary numbers of the dispersed phase and the continuous phase to characterize the different regimes of droplet generation and to predict the transition of GelMA drops to jet. Taken together, by controlling those parameters, we can control the GelMA droplet size between 30 μm to 200 μm and achieve uniform droplet size. Finally, the experiment of cell encapsulation in GelMA microgels and cell viability test results is depicted.

4.1 Materials

Experiments were carried out using materials with various viscosities, densities, and concentrations of surfactants for the continuous and dispersed phase fluids. Two different concentrations of GelMA pre-polymer solutions for the dispersed phase were prepared by dissolving 5 wt% and 8 wt% of GelMA in Phosphate Buffered Saline (PBS). Light mineral oil (high viscous material) and hexadecane (low viscous material, Sigma-Aldrich, St. Louis, MO, USA) with different concentrations, 0 wt%, 3 wt%, and 20 wt% of surfactant (Span 80, Sigma-Aldrich, St. Louis, MO, USA) were used for the continuous phase.

Gelatin methacrylate pre-polymer solution was used for the dispersed phase fluid. To prepare the GelMA pre-polymer solution, different percentages of GelMA (5 wt%, 6

wt%, and 8 wt%) were dissolved in PBS. Then, different amount of photoinitiator added to the pre-polymer GelMA solution and then final solution placed in an oven for 30 minutes at 70 ° C to be fully dissolved. Two different photoinitiators were used in this study, 0.2 wt% irgacure and 2 wt% VA-086. Each photoinitiators were mixed with GelMA pre-polymer in 15 mL centrifuge tubes, and tubes placed in the oven for 30 min at 70 ° C to be fully dissolved.

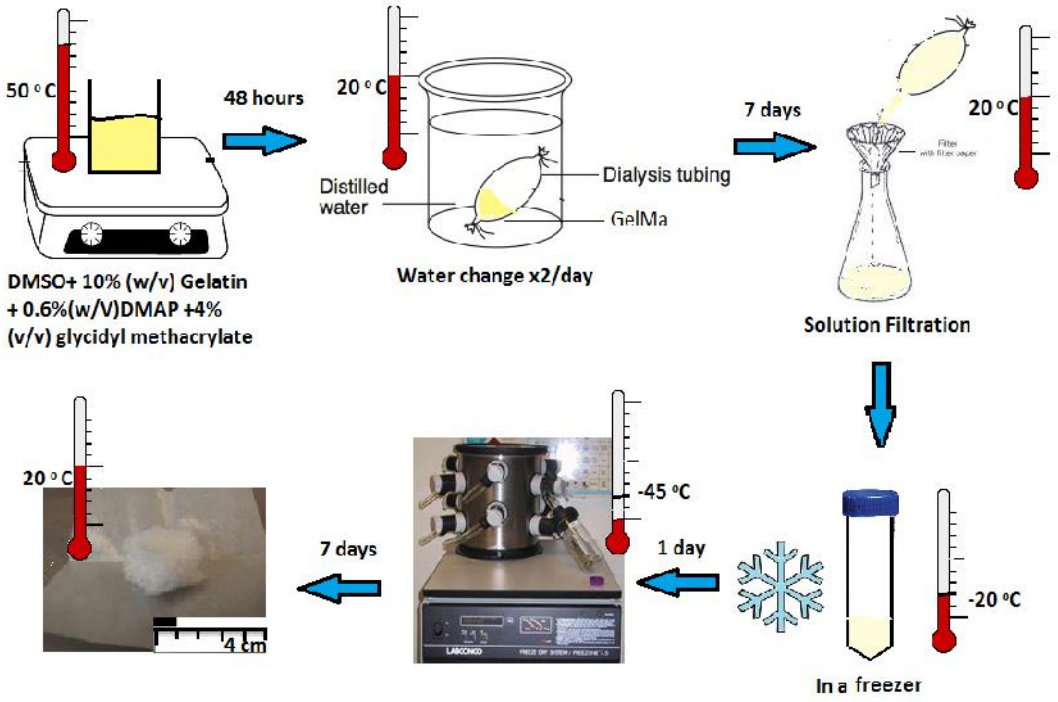

Figure 4.1 Schematic of GelMA synthesis process.

As shown in Figure. 4.1, GelMA was synthesized by the method described in [88]. Briefly, 5 g of gelatin from porcine skin (Sigma-Aldrich, St. Louis, MO, USA) was dissolved in 45 ml of dimethyl sulfoxide (Sigma-Aldrich, St. Louis, MO, USA) at 50 °C, followed by dissolving 0.5 g of 4-(dimethylamino)-pyridine (Sigma-Aldrich, St. Louis, MO, USA) in the solution. Then, 0.5 g of glycidyl methacrylate (Sigma-Aldrich, St. Louis, MO, USA) was slowly added to the solution while it was stirring at 50 °C. The reaction was kept at 50 °C for 48 hours. After that, the solution was dialyzed against

deionized (DI) water by using a dialysis membrane tube (molecular weight cut off: 12000–14000 Da; Fisher Scientific, Waltham, MA, USA) for seven days, while the deionized water was changed twice a day. Finally, the dried GelMA was made through the lyophilization process. Methacrylate group is added to make gelatin photocrosslinkable by the reaction with photoinitiators. Gelatin (denatured protein) backbone is chemically changed so as to have methacrylate groups along the backbone. The vinyl methacrylate groups allow this polymer to react either with itself or with other vinyl monomers/macromonomers to generate permanent hydrogels. This reaction can be initiated by UV. Gelatin itself becomes gel by cooling. However, this gel is not permanently crosslinked so that it becomes liquid by increasing the temperature. Gelatin has a good binding site for cell growth and thus GelMA offers a useful surface for cell attachment and growth [89].

Two different oil types were used for continuous phase: light mineral oil and hexadecane. To decrease the surface tension and prevent droplets from merging, a surfactant (Span 80) with different amounts, 3 wt%, and 20 wt%, were added to the mineral oil and hexadecane. Surfactants are organic materials that reduce the surface tension (interfacial tension) between two liquids or between a liquid and a solid. They are amphiphilic, meaning they have both hydrophilic head and hydrophobic tail groups. Surfactants are adsorbed at the interface of water and oil. The water-insoluble hydrophobic group extends out of the bulk water phase into the oil phase, while the water-soluble head group remains in the water phase. Therefore, the surface energy of the interface is reduced.

4.2 Experimental Setup and Procedure

As shown in Figure. 4.2, the flow-focusing device consists of two inlets, one outlet, a junction, an orifice channel, and an expanding chamber. The GelMA pre-polymer

solution is injected into the main inlet while oil with a surfactant is injected into the other inlet through syringes connected by plastic tubes (0.38 mm inner and 0.79 mm outer diameters). Oil flowing from two opposite sides of the channel breaks GelMA pre-polymer solution at the junction, which leads to generating GelMA droplets at the junction, the orifice channel, or the expanding chamber.

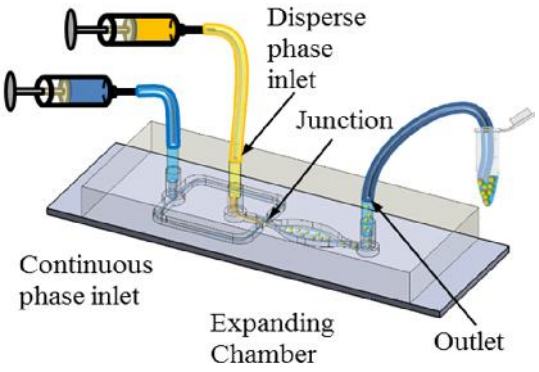

Figure 4.2 Schematic of droplet generation in a flow-focusing device

Figure. 4.3 shows the experimental setup built around a microscope, syringe pumps, a heater, and a temperature control chamber. The flow rates of both GelMA and oil are controlled by syringe pumps (KD Scientific Inc., Holliston, MA, USA). The syringe pump for injecting GelMA pre-polymer solution was placed in the temperature control chamber as GelMA tends to become a gel at room temperature. In all experiments, the flow rate of GelMA was kept constant at 2 μL/min, and the flow rate of oil was in the range of 5-40 μL/min. For the reliability of the results of each test, the device was continuously operated for 5 minutes at a constant flow rate, and then experimental data were recorded. The experiments were monitored by an inverted microscope.

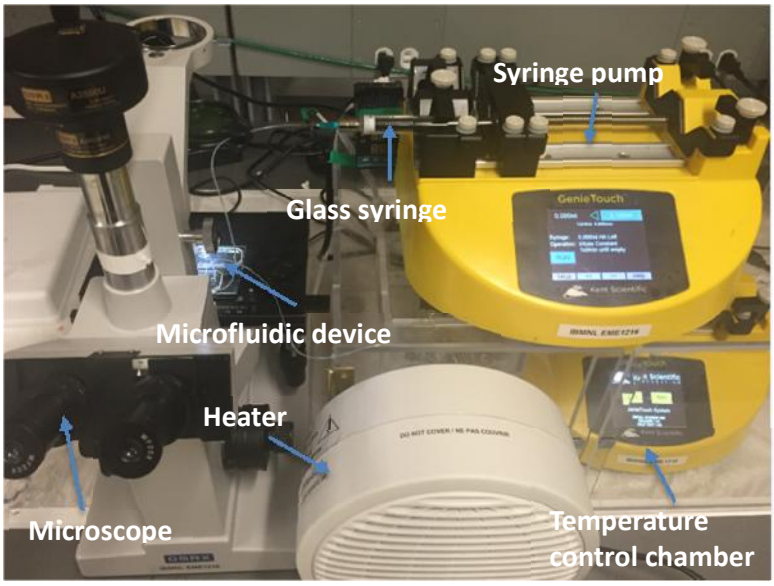

Figure 4.3 Experimental Setup

4.3 Experimental Study of Hydrogel Droplet Generation

4.3.1 Experimental Validation of Computational Simulation Results

In order to validate the computational results with experimental results, the droplet size from experimental results was compared with simulation results with the same parameters. Figure 4.4A shows the comparison of experimental and numerical results of the change in the droplet size of 5 wt% GelMA versus the various flow rates of oil with 3 wt% surfactant and Figure 4.4B shows the results of 8 wt% GelMA. As shown in these figures, the droplet size of the simulation results matches well with the droplet size of the experimental results (within 10% confidence interval). According to the Figure 4.4, there is an interval at 15 μL/min fo bth 5 and 8 wt% GelMA. This interval happened because at this flow the regime changed from the squeezing to the dripping.

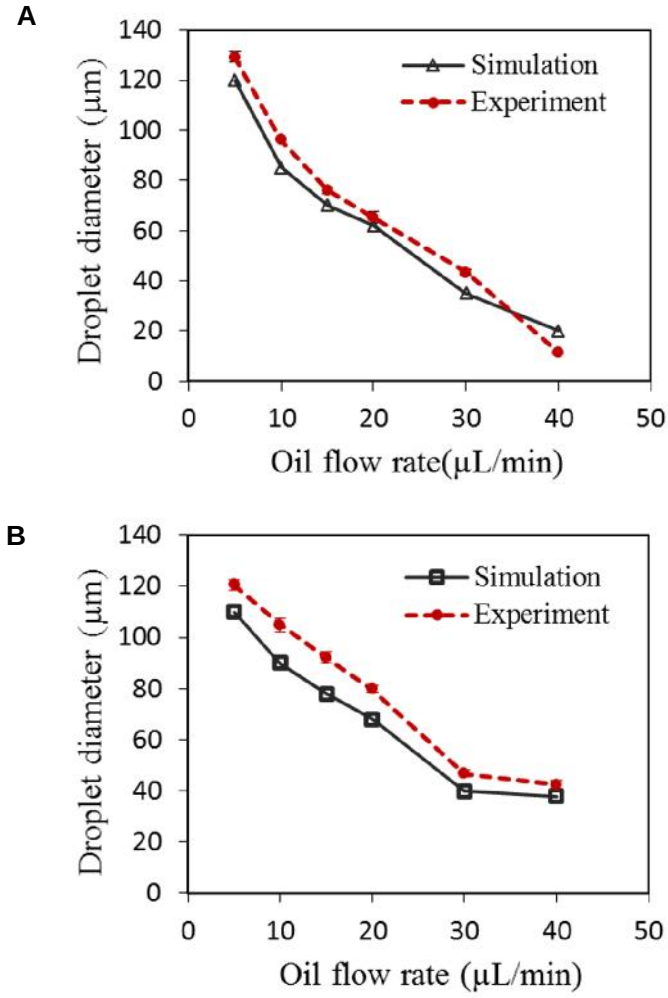

Figure 4.4 Comparison of experimental results with simulation results of the change in the GelMA droplet size. (A) Diameter of GelMA droplets (5 wt%) under the various flow rates of continuous fluid, mineral oil with 3 wt% surfactant (Span 80). (B) Diameter of GelMA microgels (8 wt%) under the various flow rate of continuous fluid, mineral oil with 3 wt% surfactant (Span 80). Flow rate of the dispersed phase (GelMA) was 2 μL/min.

Three different regimes (i.e., squeezing, dripping, and jetting) of droplet generation were demonstrated experimentally in the flow-focusing devices. Figure 4.5 shows snapshots of the droplet generation from experiments under the three regimes. In the squeezing regime experiment, 5 wt% GelMA was used for the dispersed phase and oil with 3 wt% surfactant (span 80) was used for the continuous phase. The flow rate of the dispersed phase (Qd) and the flow rate of the continuous phase (Qc) was 2 μL/min and 5

μL/min, respectively. As shown in Figure 4.5A, droplets were generated in the orifice channel. This regime occurred when the flow rate and viscosity of fluids were relatively low.

For the dripping regime experiment, 5 wt% GelMA was used for the dispersed phase and oil with 3 wt% surfactant (Span 80) was used for the continuous phase. The flow rate of the dispersed phase (Qd) and the flow rate of the continuous phase (Qc) was 2 μL/min and 20 μL/min, respectively. The flow rate of the continuous phase was much greater than the dispersed phase. As shown in Figure 4.5B, the droplets were cut off because the viscosity of the continuous phase fluid overcame the interfacial force of the dispersed phase and the size of droplets was smaller than the width of the orifice channel. In this case, droplets broke because of Rayleigh-Plateau instability [90]. Both squeezing regime and dripping regime experiment results were well matched with computational simulation results described in Chapter 3.3.

In the jetting regime (shown in Figure 4.5C), the thin stream of the dispersed phase was created, and droplets were finally cut off in the expansion chamber as a result of Rayleigh-Plateau instability. This regime occurred when the viscosity of the continuous and dispersed phases were both high. Therefore, 8 wt% GelMA was used for the dispersed phase and oil with 20 wt% surfactant (Span 80) was used for the continuous phase. The flow rate of the dispersed phase (Qd) and flow rate of the continuous phase (Qc) was 2 μL/min and 40 μL/min respectively. The viscosity of the continuous phase dragged the dispersed phase, but the formation of the droplets was suppressed because of the high viscosity of the dispersed phase, resulting in the jetting regime.

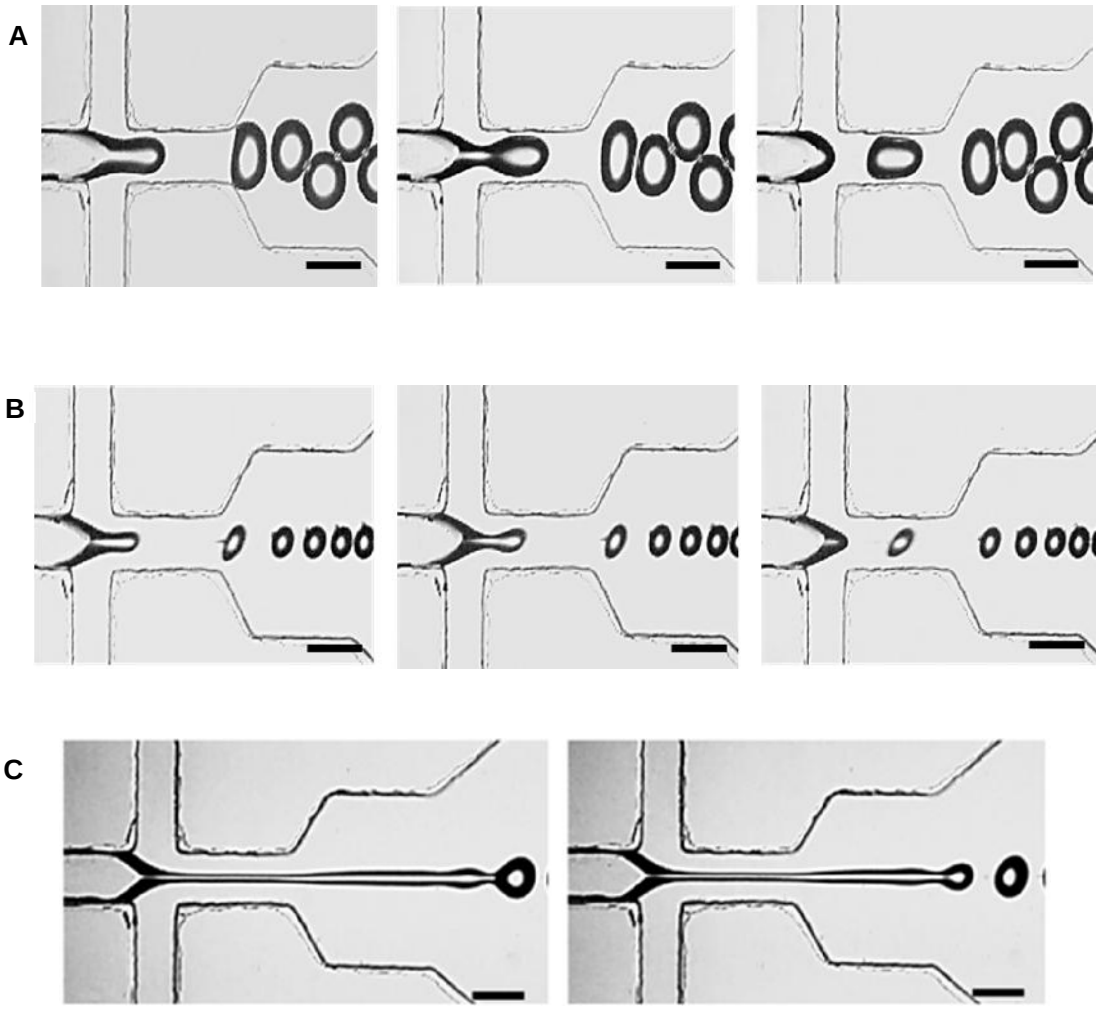

Figure 4.5 Representative snapshots of droplet generation during (A) the squeezing regime, (B) the dripping regime, and (C) the jetting regime. Scale bar = 100 µm.

4.3.2 Various Parameters for Controlling Droplet Size

In order to study the effect of surface tension on droplet generation, hexadecane and mineral oil without surfactant were compared with hexadecane and mineral oil with 3% surfactant (Span 80). By adding surfactant up to 3% to the fluid, the surface tension of the continuous phase liquids was dramatically decreased. However, it did not change the viscosity of the liquids.

The diameters of the droplets created by mineral oil and hexadecane, with different percentage of surfactant, are shown in Figure 4.6. Comparing the results of hexadecane without surfactant, hexadecane with 3% surfactant, mineral oil without surfactant, and mineral oil with 3% surfactant shows that when surface tension between two immiscible fluid drops, the size of droplets were decreased. In addition to the effect of surfactant on decreasing the size of droplets, uniform monodisperse droplets were dependent on the existence of the surfactant in the continuous phase. As shown in Figure 4.7A, droplets that were created without the surfactant were easily merged after generation, resulting in non-uniform droplet sizes. However, uniform monodisperse droplets were created by adding surfactants (Figure 4.7B).

In order to study the effect of the dispersed phase viscosity (GelMA concentration), two different solutions of GelMA 5 wt% (Figure 4.6A and C) and 8 wt% (Figure 4.6B and D) were carried out. It was found that the generated droplet diameters were very sensitive to the concentration of GelMA. Comparing the cases with the same continuous phase, but different GelMA concentrations (as their dispersed phase), it was found that droplet size increases by increasing the GelMA concentration. This suggests that the size of the droplet does not only depend on the viscosity of a continuous phase but also depends on GelMA concentration. In addition, the jetting regime observed, when GelMA 8 wt% and mineral oil with 20 wt% surfactant (for the dispersed phase and the continuous

phase, respectively) were used, due to the high viscosity of the continuous phase fluid and dispersed phase fluid (Figure 4.6D).

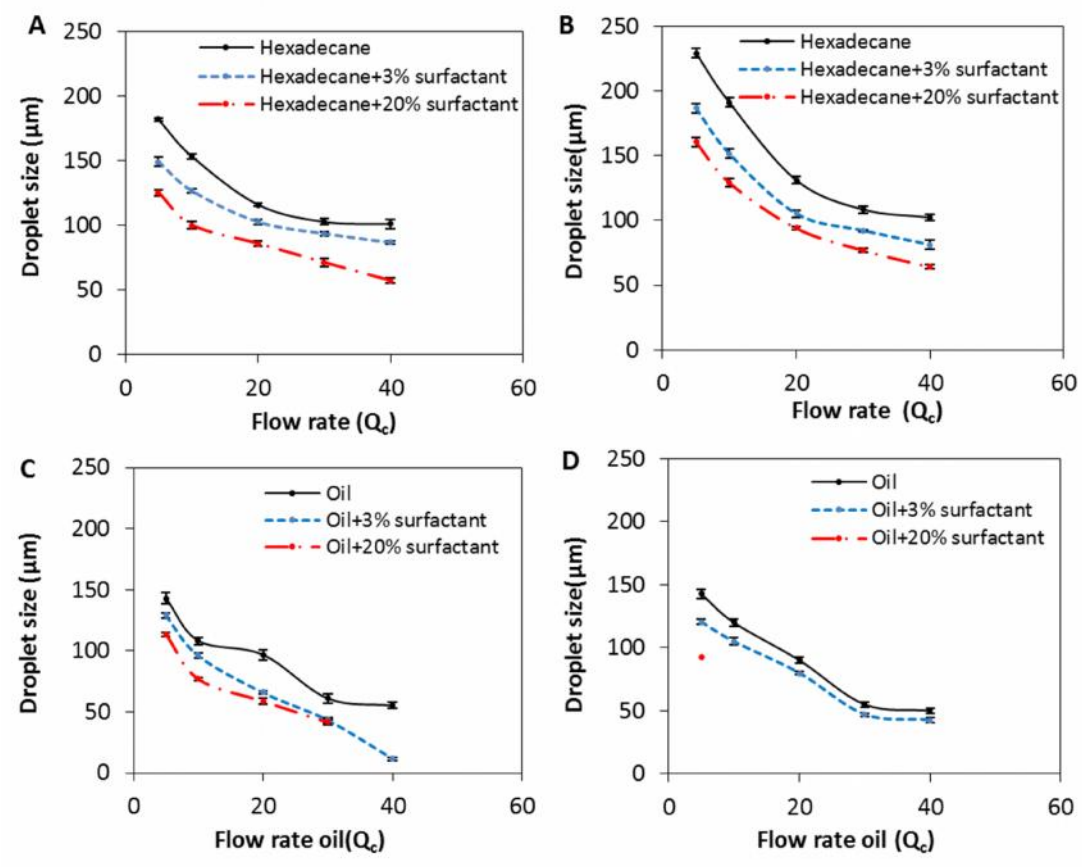

Figure 4.6 GelMA droplet sizes versus various flow rate of oil. (A) 5 wt% GelMA was used for the dispersed phase and Hexadecane with different concentrations of surfactant was used for the continuous phase. (B) 8 wt% GelMA was used for the dispersed phase and Hexadecane with different concentrations of surfactant was used for the continuous phase. (C) 5 wt% GelMA was used for the dispersed phase and mineral oil with different concentrations of surfactant was used for the continuous phase. (D) 8 wt% GelMA was used for the dispersed phase and mineral oil with different concentrations of surfactant was used for the continuous phase. The number of measurement for droplet size is five and standard deviation is shown for five droplets in each cases.

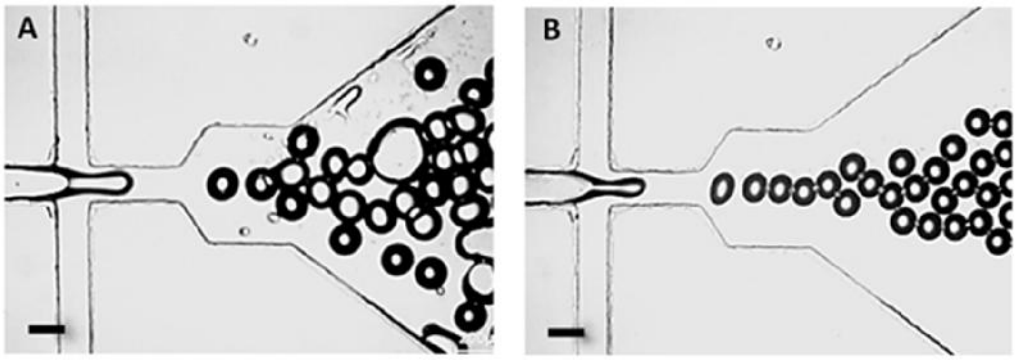

Figure 4.7 Effect of surfactant for the droplet generation. 5 wt% GelMA was used for the dispersed phase with two different solution for the continuous phase: (A) mineral oil without surfactant (B) mineral oil with 3 wt% surfactant. Flow rate of GelMA and flow rate of the continuous phase was 2 µL/min and 10 µL/min, respectively. Scale bar = 100µm.

Using a higher concentration of GelMA makes the inertia force of the dispersed phase to be considerable, which results in creating a jetting regime. In this study, the flow rate of hydrogel pre-polymer solution kept constant at 2 µL/min in order to prevent the formation of the jetting regime. At higher flow rates of hydrogel pre-polymer solution, the inertia force of dispersed phase fluid (hydrogel pre-polymer solution) becomes dominant and the Webber number of disperse phase is more than (We >1), resulting in a stream of the jet.

The effect of viscosity of the continuous phase was studied by comparing cases of mineral oil and hexadecane with 3% surfactant (µ = 4.2 mPa·s) and 20% surfactant (µ = 6.7 mPa·s). Adding more than 3% surfactant to the fluid will not change the interfacial tension between the dispersed phase fluid and the continuous phase fluid because of the micelle effect [91]. However, it increases the viscosity of the fluids dramatically. Figure 4.6A and B showed droplet sizes when hexadecane was used as a continuous phase. Comparing hexadecane with 3% surfactant and 20% surfactant shows that the size of the droplets was decreased by increasing the viscosity of the continuous phase (the amount of surfactant). Also, the same results are shown by comparing the mineral oil and

hexadecane (Figure 4.6), since the viscosity of hexadecane is much less than mineral oil while the surface tension of mineral oil and hexadecane is almost the same. In addition, the high viscosity of the continuous phase fluid caused the dispersed phase fluid to stretch into long thin streams. At the high viscosity of the continuous phase, it is difficult to fabricate 8 wt% GelMA droplet. However, a higher concentration of GelMA is required for fabricating stiffer microgels in tissue engineering applications. In addition, UV exposure time to crosslink the hydrogel is decreased with a higher concentration of GelMA, resulting in higher cell viability for cell-laden hydrogel application. According to Figure 4.6, small 8 wt% GelMA droplets could be created when less viscous continuous phase fluid (e.g. hexadecane) was used. When hexadecane used as a continuous phase, due to the low viscosity of the hexadecane, GelMA droplets of two different concentrations (5 wt% and 8 wt%) were created through the squeezing regime. These results show that hexadecane could be a good option for fabricating high concentration of hydrogel droplets in tissue engineering application. Moreover, hexadecane presents high biocompatibility using as a continuous phase for fabricating cell-laden alginate droplets [41].

Figure 4.8 shows the effect of the flow rate for the continuous phase. The sizes of the droplets were dramatically decreased by increasing the flow rate of a continuous phase. By increasing the flow rate of the continuous phase, the viscosity of the continuous phase increased, thus, the high viscosity of the continuous phase suppressed the dispersed phase fluid, resulting in the small size of droplets.

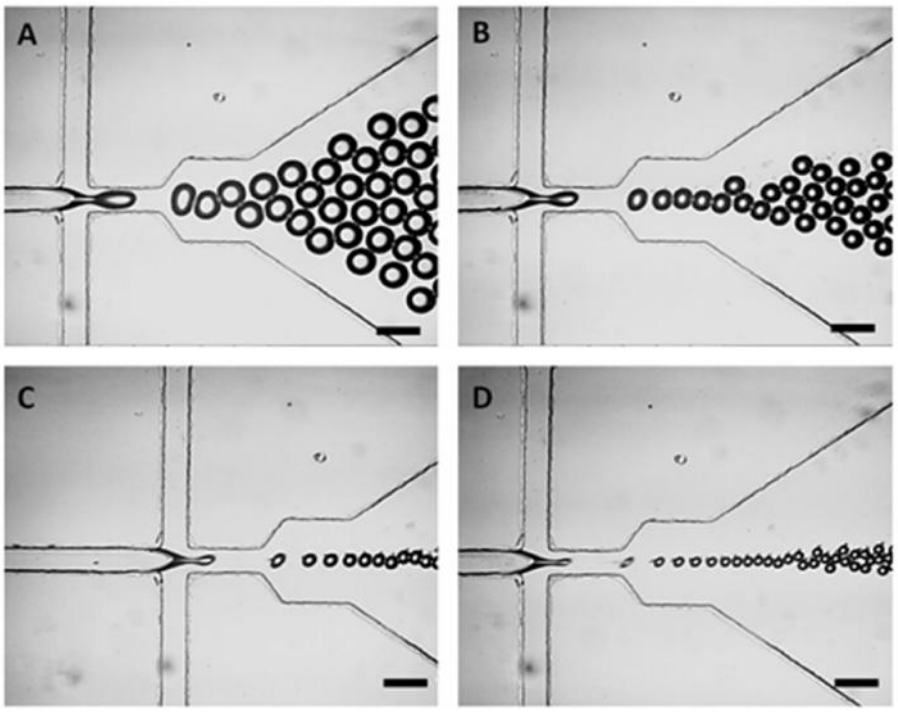

Figure 4.8 GelMA microgels generation in flow-focusing device under various flow rate of the continuous phase, (A) Qc = 5 µL/min, (B) Qc = 10 µL/min, (C) Qc = 20 µL/min, and (D) Qc = 30 µL/min. 5 wt% GelMA was used for the dispersed phase and mineral oil with 3 wt% surfactant (Span 80) was used for the continuous phase. Flow rate of dispersed phase was Qd = 2 µL/min. Scale bar = 200 µm.

4.3.3 Characterization of Hydrogel Droplet Generation Regime

Figure 4.9 shows a phase diagram of GelMA droplet generation observed through the experiments. Capillary numbers of each experiment were calculated and plotted on the phase diagram to predict the formation of GelMA droplets or a jet stream in a flow-focusing device. In flow-focusing geometry, non-dimensional capillary numbers are important in describing the transition between the dripping and the jetting regime, because the viscosity of the flow-focusing devices. The capillary number of the continuous phase $Ca_c = \mu v/\sigma$ and disperse phase $Ca_d = \mu v/\sigma$ described in Figure 4.9 shows the range of formation of each regime.

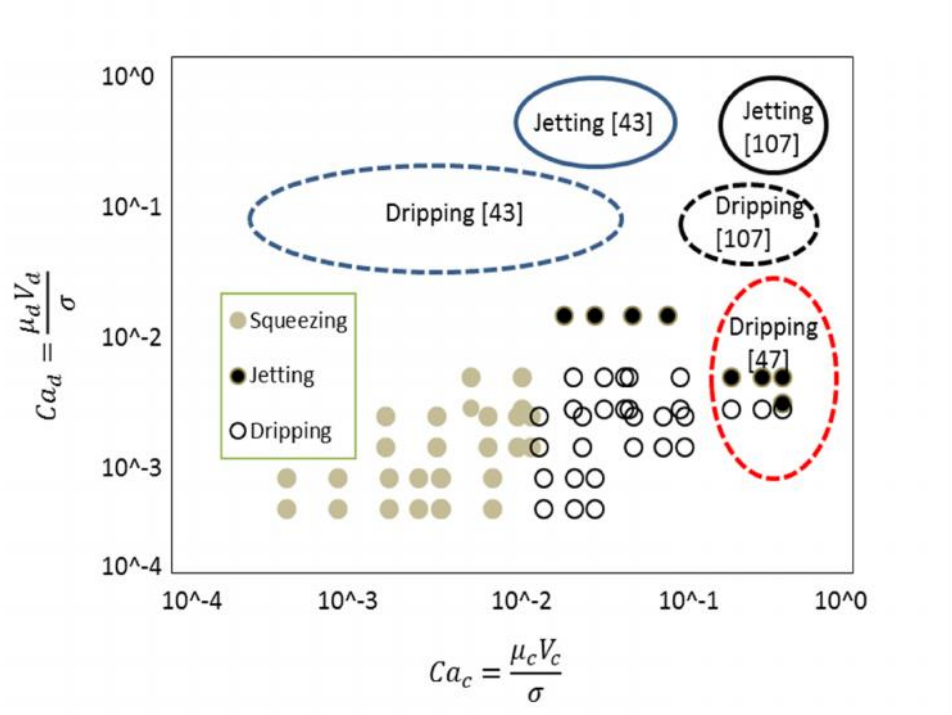

Figure 4.9 A phase diagram shows three different regimes resulting from the flow-focusing device in comparison with previously reported results.

The result shows that at very low capillary numbers of continuous ($Ca_c<10^{-2}$) and dispersed phase fluids ($Ca_d<10^{-2}$), the squeezing regime happens, and droplets are created at a size bigger than the width of the channel. When $10^{-2}<Ca_c<10^{-1}$ and $Ca_d<10^{-2}$, the dripping regime happens, and the droplets are created at a size smaller than the width of the channel. At high capillary numbers of continuous phase fluid ($10^{-1} <Ca_c< 10$) and $Ca_d>10^{-2}$, the thin jet stream of the dispersed phase fluid is created. The results show that the transition from the dripping regime to the jetting regime happens at $Ca_c \sim 10^{-1}$.

The capillary numbers of jetting and dripping regime observed from different studies, water in oil droplets, are also shown in the phase diagram. According to the results in [44] [92] [48], most of the capillary numbers of the dispersed phase in the experiments were in the range of $Ca_d > 10^{-2}$ for both dripping and jetting regime. However, the results of our experiment shows that due to the high viscosity of hydrogels (the viscosity of 5 wt%

GelMA = 2.8 mPa·s and 8 wt% GelMA = 4.9 mPa·s), the GelMA prepolymer droplets are not created at $Ca_d > 10^{-2}$. At $Ca_d > 10^{-2}$ only the jetting regime of GelMA is created.

Therefore, the results from the previous studies for droplet generation of water in oil is not applicable for hydrogel droplet generation for tissue engineering application. This phase diagram provides a comprehensive study of hydrogel droplet generation in tissue engineering application.

4.4 Cell Encapsulation Experiments

4.4.1 Cell Culture

NIH-3T3 mouse embryonic fibroblasts were cultured in Dulbecco's modified Eagle's medium (Invitrogen, Carlsbad, CA, USA) supplemented with 1% penicillin-streptomycin (Invitrogen, Carlsbad, CA, USA) and 10% fetal bovine serum (Invitrogen, Carlsbad, CA, USA) at 5% CO_2 and 37 °C. When cell proliferation rates reach around 80-90% confluency (Figure 4.10A), cells were passaged into new flasks. Old media was aspirated, and 5 ml of PBS was used to wash out the flask twice to remove floating dead cells. 3 mL of trypsin was used to detach the cells from the flask for 3 minutes inside the incubator. The trypsin was then deactivated with 9 mL of fresh media. The mixture of cells, trypsin and media were centrifuged at 1400 rpm for 2 minutes. The liquid phase was aspirated, and a cell pellet was suspended in 3 ml of new media. Suspended cells were seeded in flasks for culturing. The same protocol was used to culture MCF-7 breast cancer cells. However, the media used for MCF-7 cells were DMEM supplemented with 1% penicillin-streptomycin, 10% fetal bovine serum (FBS), and 1% fungizone. MCF-7 breast cancer cells cultured in a flask are shown in Figure 4.10B.

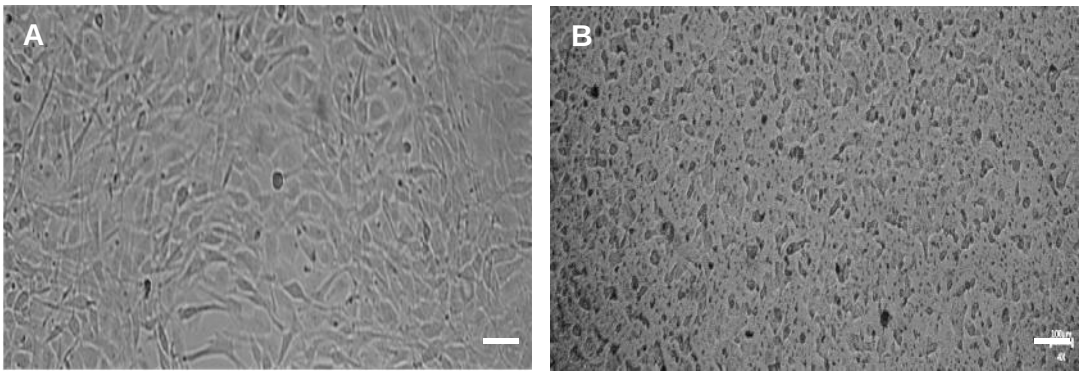

Figure 4.10 Cells are cultured and confluent in flasks (A) NIH3T3 fibroblast and (B) MCF-7 breast cancer cells show different behavior. Scale bar = 100 µm.

4.4.2 Materials and Experimental Procedure

For a cell encapsulation experiment, two different types of cells (NIH 3T3 fibroblast and MCF-7 breast cancer cells) were detached from the flask and resuspended in the GelMA pre-polymer solution. 6 x 10^6 cells/mL of MCF-7 cells were mixed with 5 wt% GelMA pre-polymer solution and 0.5 wt% 2-Hydroxy-4′-(2-hydroxyethoxy)-2-methylpropiophenone (Sigma-Aldrich, St. Louis, MS, USA) as a photoinitiator (PI 1). Also, 6 x 10^6 cells/mL of 3T3 fibroblasts were mixed with a 5 wt% GelMA pre-polymer solution and 2 wt% 2,2'-Azobis[2-methyl-N-(2-hydroxyethyl)propionamide (VA-086, Wako Pure Chemical Industries, Ltd., Japan) as another photoinitiator (PI 2). GelMA pre-polymer solution mixed with cells were used as a dispersed phase and mineral oil with 20 wt% surfactant was used as a continuous phase. The flow rate of the dispersed phase applied to GelMA pre-polymer solution with cells was in the range of 0.3-1 µL/min and the flow rate of continuous phase was in the range of 0.8-3 µL/min. Since adding cells in the GelMA increased the viscosity of the solution, the low flow rate of dispersed and continuous phase had to apply to avoid the increment of capillary numbers.

Cell-laden GelMA pre-polymer droplets were created in a flow-focusing device (Figure 4.11) and were exposed to UV light at 365 nm and intensity of 4 mW/cm^2 for photocrosslinking. The photocrosslinking process allows the spatial and temporal control of the hydrogel formation [93]. Therefore, as the concentration of photoinitiator is increased, the crosslinking time of GelMA is decreased. However, the amount of photoinitiator and UV exposure time to crosslink affect cell viability. Optimizing the minimum amount of photoinitiator and shortest crosslinking time is critical for cell viability. This study found that the minimum amount of 2-Hydroxy-4′-(2-hydroxyethoxy)-2-methylpropiophenone (PI 1) to crosslink 5 wt% GelMA was 0.5 wt% with 7 minutes UV exposure time. The minimum amount of VA-086 (PI 2) to crosslink 5 wt% GelMA was 2 wt% with 5 minutes UV exposure time. Although these photoinitiatores crosslink the GelMA prepolymer at short wave length (254 nm) in less than 5 min, the GelMA prepolymer was exposed to UV at long wave length (365 nm) for longer time in order to decrease the cell damage. Because the shortwave length of UV effects on cell viability.

The GelMA droplets containing fibroblast cells generated in the flow-focusing device were collected in 1.5 mL centrifuge tubes and crosslinked by UV exposure for 7 minutes. Also, GelMA droplets with MCF-7 cells were crosslinked by 5 minutes UV exposure. The surfactant and oil were separated from the cell-laden GelMA microgels using a centrifuge at 10000 rpm for 5 minutes. The centrifugation process was repeated two times to make sure all the oil and surfactant were removed from the cell-laden GelMA microgels.

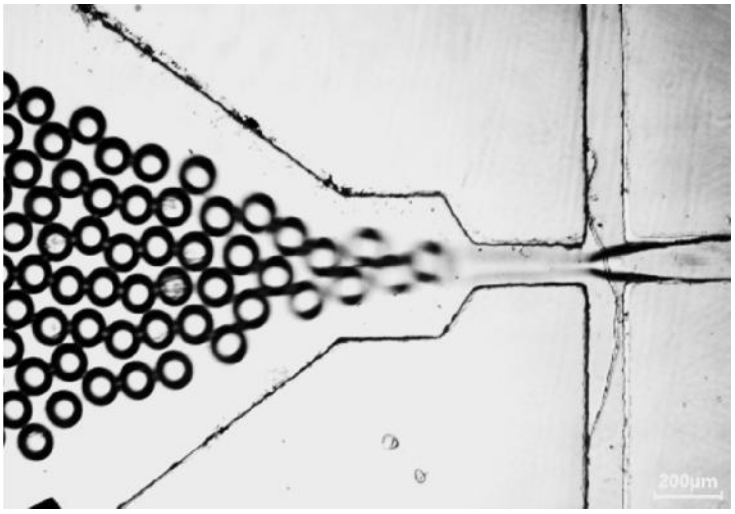

Figure 4.11 Cell laden droplet generation (100-150 µm in diameter). 6 x 10^6 cells/mL of MCF-7 breast cancer cells were mixed in 5 wt% GelMA and 2 wt% VA-086 photoinitiator. Scale bar = 200 µm

4.4.3 Assessment of Cell Viability

To examine the cell viability, the cell-laden microgels were stained with a Live/Dead cell viability assay (Invitrogen, Carlsbad, CA, USA). The assay consists of two fluorescence dyes, calcein acetoxymethyl (Calcein AM) and ethidium homodimer III (EthD-III), for staining both live and dead cells and measures two recognized parameters of cell viability such as intercellular esterase activity and plasma membrane integrity. Calcein AM, which is a permeable and fluorescent reagent, is converted to the intensely green fluorescent calcein by the intracellular esterase [94]. EthD-III enters into cells through the damaged membrane, producing a bright red fluorescence signal when binding to nucleic acids. EthD- III is excluded by the intact plasma membrane of live cells.

Dye concentrations are required to adjust to achieve distinct labels of live cells with Calcein-AM and of dead cells with EthD-III. The optimal concentration of dye is different for different cell types. However, it is best to use the lowest dye concentration that gives a sufficient signal. The standard staining solution is prepared as follows;

1- Calcein-AM and EthD-III stock solutions are removed from the freezer and allowed to warm at room temperature for 30 min.
2- 4 µL of EthD-III and 2 µL of Calcein-AM are added to 2 mL PBS.
3- The stock solution is vortexed to ensure complete mixing of two dyes and keep in a refrigerator before use.

200 µL of stock solution of the live/dead assay was added to a 1 mL tube with cell-laden GelMA microgels, and then the tube was incubated at 37 ^{o}C and 5% CO_2 for 30 minutes. The cell-laden microgels in the tube were washed with PBS three times to remove the excessive assay solution. The cell-laden microgels were examined under a fluorescent microscope (FLUOVIEW FV1000, Olympus, Japan) to check cell viability. Figure 4.12 shows fluorescently labeled NIH 3T3 cells encapsulated in a GelMA microgels with PI 1.

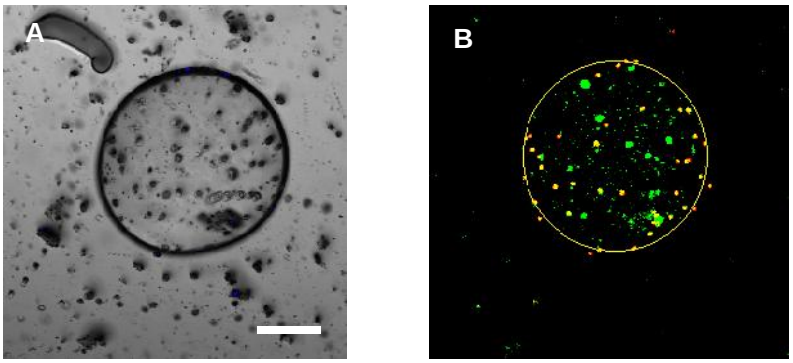

Figure 4.12 NIH 3T3 fibroblast cells encapsulated in a microgel. (A) A phase contrast image and (B) live/dead assayed image. Both were taken from a confocal microscope at day 0. Scale bar = 50 µm.

Figure 4.13 shows fluorescently labeled MCF-7 cells encapsulated in GelMA microgels with PI 2. As shown in Figure 4.14, the cell viability analysis of MCF-7 (~90 %) is higher than NIH 3T3 (~80%). The possible reason is that PI 2 with shorter UV time is more biocompatible than that of PI 1 with longer UV time. However, a further experimental investigation will be required in future works.

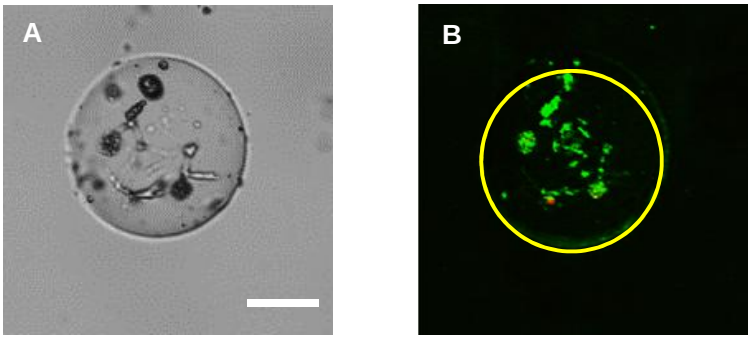

Figure 4.13 MCF-7 breast cancer cells encapsulated in a microgel. (A) A phase contrast image and (B) live/dead assayed image. Both were taken from a confocal microscope at day 0. Scale bar = 50 µm.

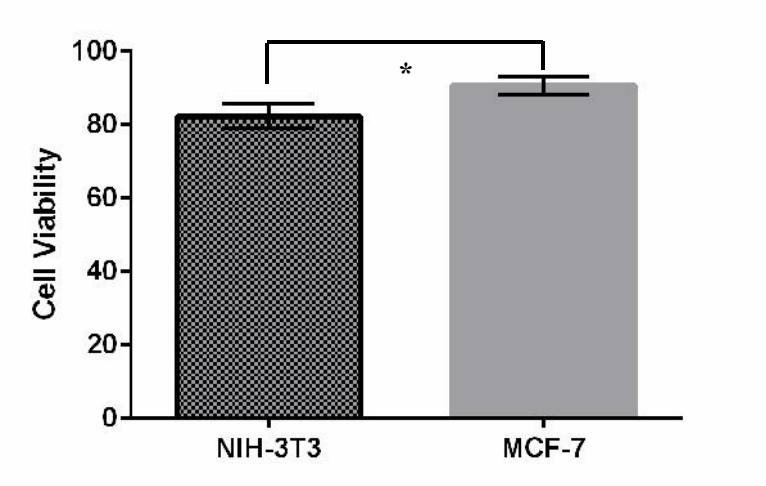

Figure 4.14 Cell viability analysis. (n=5 microgels, Error bar: Standard Deviation, ****P*-value < 0.05).**

4.5 Summary

The experimental study of GelMA pre-polymer droplet generation was described in this chapter. GelMA pre-polymer solution with various concentrations was used as a dispersed phase and light mineral oil and hexadecane with different amounts of surfactant were used as a continuous phase to study the effect of various parameters on droplet generation in a flow-focusing device. Experiments were carried out with various flow rates of the oil and hexadecane and constant flow rate of GelMA pre-polymer solution to

characterize the effect of continuous viscous force on the droplet size. Experimental results showed that the flow rates of the continuous phase controlled the size of GelMA pre-polymer droplets and created squeezing, dripping, and jetting regimes. All the parameters were summarized into a non-dimensional capillary number which defines the effect of continuous viscous force and interfacial force on GelMA pre-polymer droplet generation. A phase diagram of capillary numbers of the dispersed phase versus continuous phase was plotted to place different regimes of generating GelMA pre-polymer droplets with different conditions. The results show that the transition from the dripping regime to the jetting regime happens at $Ca_c \sim 10^{-1}$. Finally, GelMA microgels encapsulating two types of cells were fabricated, and the viability of cells encapsulated in GelMA microgels was tested using the Live/Dead cell viability assay. Cell viability of higher than 80 % was achieved in this study.

Chapter 5 Fabrication of Circular Channel Microfluidic Devices

In chapter 2, the fabrication method of flow-focusing microfluidic devices was described. With the conventional microfabrication method, the cross-section of the microchannel is limited to a rectangular shape. Droplet generation using the rectangular channel devices has drawbacks that are explained in details in the introduction of this chapter. To address these problems, this study developed a method to fabricate a circular microchannel flow-focusing device. This circular cross-section flow-focusing device could be used for droplet generation to generate more uniform droplets. The fabrication process as well as results of droplet generation using this device is presented in this chapter.

5.1 Overview

A photolithography microfabrication method [95] has been used to fabricate a master mold to cast microfluidic channel devices for droplet generation. However, the cross-sectional shape of the channels fabricated by the photolithography technique is limited to a rectangular shape. The rectangular channel has several drawbacks to generate droplets [96]. In the rectangular channel, the dispersed phase fluid wets the top and bottom walls at a low flow rate of continuous phase fluid. Wetting walls have two disadvantages: (1) cells mixed in dispersed phase tend to attach to the walls or are damaged because of shear force at the surface [97]; and (2) capillary instability is changed and in the result droplet break up is not controllable [98][99]. By increasing the flow rate of a continuous phase, the wetting surface of dispersed phase might be eliminated; however, another problem occurs, such as device leaking and cell damage because of high shear force. Another important factor in droplet generation is the uniformity of droplets. To generate uniform droplets, a uniform velocity profile in the cross-sectional direction is required. Since the circular microfluidic channel is truly symmetrical unlike the rectangular cross-sectional

channel, it can generate the uniform velocity profile in the cross-sectional direction [100]. Circular channels that squeeze the dispersed fluid in all direction prevent dispersed fluid to wet the walls. This results in creating well controllable, monodisperse droplets. Also, rectangular channels are more likely to clog due to aggregation of synthesized droplets [101].

Due to these disadvantages, alternative fabrication methods have been developed to fabricate circular channels. For example, one method involves a trench imbedded in a silicon wafer. The trench is then filled with a thick layer of doped silicon oxide, followed by heating, which closes the trench, and creates a circular channel [102]. However, this technique is able only to fabricate small-sized silicon channels (a few micrometers in diameter). Another method for making circular channels utilized the capillary rise of liquid PDMS inside an open channel in a PDMS slab [103]. This method is not practical for fabricating circular channels smaller than 100 μm. Abdelgawad *et al*. introduced a new method of fabricating circular channel by injecting liquid PDMS through a rectangular channel, fabricated by the microfabrication softlithography method, followed by passing air stream in a channel filled with liquid PDMS [96]. PDMS injection fills the corner of the rectangular channel which can make a simple circular channel. In addition to these methods, standard fabrication methods such as three dimensional (3D) printing [104][105], micro-cross construction [106] and laser machining [107] have also been used for fabricating circular channels. Also, the circular microfluidic channel was created using the combination of micromolding and softlitoghraphy [108] and photolithographic reflowable photoresist [109]. The mold fabrication using these methods often requires many processing steps. Among these methods, due to the emergence of high resolution 3D printers, 3D printing provides a simple and efficient tool for creating the molds (with

micro-sized features) that can be used for fabricating microfluidic channels with circular cross section.

Recently, 3D printing has been used to fabricate circular microfluidic channels for flow focusing applications [110]. However, the fabricated circular channels were not perfectly circular. Therefore, although the resolution of 3D printing has increased, creating a perfect circular microfluidic channel for a micro droplet generation remains challenging. In this chapter, a fast, low cost technique is presented for fabricating circular channel flow-focusing microfluidic devices using a 3D printing method. Challenges regarding the use of 3D printed molds in the peel-off process, removing cloudy surface finishes in the castings, getting fully circular geometries, and fixing misalignment have been addressed. The flow-focusing channels are used to generate hydrogel droplets ~200 µm in diameter, with the diameter of the droplet being controlled by the flow rates of the fluid [111].

5.2 Methods for Circular Microchannel Fabrication

5.2.1 Mold Fabrication Using a 3D printer

The mold is designed using SolidWorks® (Dassault Systems, Vélizy-Villacoublay, France) software. Two identical molds are designed with similar geometry except for the alignment pins. The male and female alignment features are made so that the two halves of the microfluidic chip would align as desired [110]. An STL format of the mold is then printed (see Figure 5.1A) with a poly jet 3D printer (Object500 Connex, Stratasys Ltd., Eden Prairie, USA) using VeroWhite-FullCure®830 (Stratasys Ltd., Eden Prairie, USA) materials at 16 µm layer resolution in Z direction and 45 µm build resolution in X-Y direction. The molds were fabricated with a glossy surface finish to allow a smooth surface with the roughness (Rz) of 3.8 µm previously reported in [112]. After printing,

the mold is baked at 80□C overnight. The part is then silanized with Trichloro (1H,1H,2H,2H-perfluro-octyl) silane (Sigma-Aldrich, St. Louis, USA). Salinization is performed by adding 50 µL of the silane solution to a petri dish and placing the petri dish and the molds into a desiccator for 30 minutes. These processes are necessary to easily peel the cured PDMS channel from the mold made of the VeroWhite material [113].

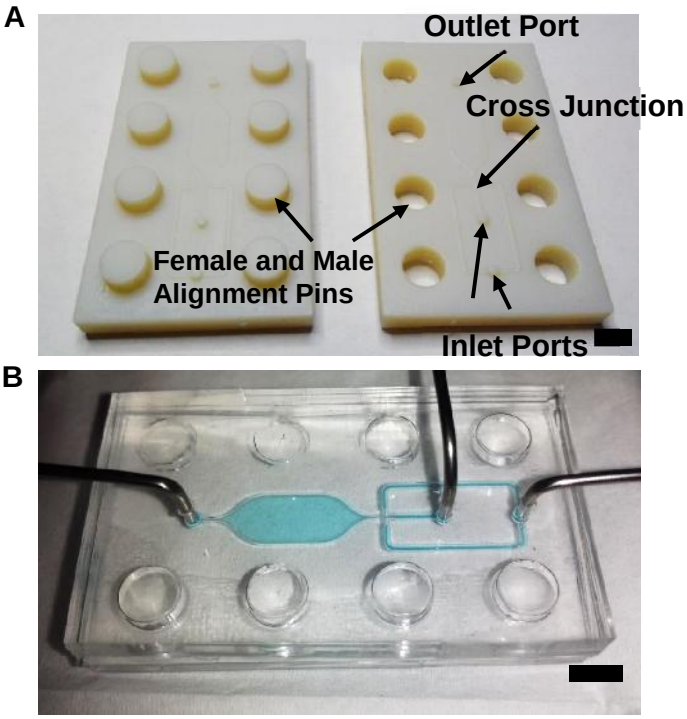

Figure 5.1 Device fabrication using 3D printed molds. (A) SolidWorks rendering of 3D modeled molds for the microfluidic chip castings with features labeled. (B) Assembled microfluidic chip with light blue dye shows channels with no leakage observable. Scale bar = 5 mm.

5.2.2 PDMS Casting

The casting process creates the two halves of the microfluidic channel device with their internal geometries. It is important that the reusable molds are first properly prepared by cleaning the surface with isopropanol to ensure that the surface is particle and residue free. The two halves of the microfluidic chip are made by pouring the liquid PDMS

(SYLGARD 184, Dow Corning Co., Midland, USA) over the molds in a petri dish. The PDMS is made of an elastomer and a curing agent mixture with a 10:1 ratio. Once the liquid mixture is poured, it is placed in a desiccator for approximately 90 minutes or until all the bubbles have dissipated. The mold is then placed in an oven at 70 °C for three hours to solidify the PDMS. Once the PDMS has cured, it can be peeled from the petri dish and mold.

5.2.3 Device Bonding

The procedure for assembling the two halves of the microfluidic parts into a chip are as follows. First, the holes for the inlet and outlets are cut using a punch. To get a strong bond between the two halves of the microfluidic chip, the surfaces of both chips must be clean. To clean the PDMS parts, they are placed in an ultrasonic bath with reverse osmosis water for approximately 5 minutes. When the parts are dry, they are exposed to a handheld corona device (BD-20, Electro-Technic Products, USA) for 5 minutes (at 30 seconds/cm^2) which is necessary to achieve a strong bond [75]. Finally, the two halves are put together and clamped for 72 hours to allow the bond to cure. The bonding of the device is checked with the injection of colored liquid shown in Figure 5.1B.

5.2.4 Liquid PDMS Injection

To obtain circular channels, a PDMS injection coating method [96] is adopted. A 2:1 liquid heptane/'PDMS mixture is injected into the microfluidic chip, and then allowed to cure while an air stream flowed through the channels. The PDMS is the standard 10:1 base to curing agent ratio. After the heptane/PDMS is fully injected into the internal geometries of the chip, the chip is placed on a hotplate for 60 seconds at 100°C. After 60 seconds, air is pumped into the chip at a constant flow rate of 24 mL/min. Air is pumped into all inlets and allowed to escape through all outlets. It is important that the air is

forced through all the channels to prevent blockages in the device. The chip should remain on the hotplate, with constant air flow, for 10 minutes. This process can be repeated to obtain smaller diameter channels with slight variations to curing times, baking temperatures and air flow volumes. Circular channels ranging from 200 µm to 5 µm were successfully fabricated by Abdelgawad *et al.* [96].

5.3 Result and Discussion

The fabrication process explained in the previous section was used to fabricate a circular channel microfluidic flow-focusing droplet generator. The half circular channels were fabricated in PDMS, and bonded to each other. If the PDMS is not fully cured (where it is in contact with the mold), it could indicate that the VeroWhite material was interfering with the curing process. As mentioned in the previous section, this problem can be mitigated by baking and silanizing the mold. Another potential problem with casting is a cloudy or rough surface finish. This can be mitigated by ensuring the mold is free of any residue. In addition, the curing temperature during the casting process has the potential to warp to mold. Therefore, to decrease the chance of warping the mold, it is important to keep any temperature during casting below 70°C.

As shown in Figure 5.1B, the two parts were successfully attached to each other, and no leakage was observed. Acceptable bonding strength between the two halves of this microfluidic chip can be difficult to obtain consistently. Thus, it is important that the surfaces between the two halves of the microfluidic chip are in full contact with one another. Warped molds, or casting the PDMS on uneven surfaces, can lead to problems with achieving full surface contact. Using a clamp is a good way to ensure full contact. The bond was found to be strong enough to carry out experiments without any leakage from the channels shown in Figure 5.1B.

Due to the limitations of the 3D printer, the ~200 µm channels fabricated using the 3D printed molds were elliptic shaped as opposed to the desired circular. Figure 5.2A shows a cross section of the PDMS channel after the assembly. As can be seen, the width of the individual channel was extended and the depth of the channel was too shallow. The channels were elliptic shaped with pointed edges where the two halves of the PDMS join together. This problem was caused by the limitations of printing at the micro scale, as the printer material cannot hold the desired half circle shape and collapses into the "mound" shape. Even 3D printers with high resolution were not able to fabricate sharp edge of the half circular channel. In result, a perfect circular channel was not created after bonding two PDMS halves. Therefore, a post PDMS injection was required to cover misalignment and create a fully circular channel. To achieve circular channels, we injected the liquid PDMS solution and cured it by pumping air flow through the channels described in the method section. A common problem associated with this process was the air not reaching all of the outlets. Air can create a path to one outlet, and not make a path to another. A simple fix was to plug the outlet that has the path, and to force the air to the other outlet. Once a path has been formed by the air to all outlets, it is important that air is allowed to flow freely through all of them. If air is not allowed to flow through a channel, the PDMS will cure, and block the entire channel. Post PDMS injection coating yields results were shown in Figure 5.2B.

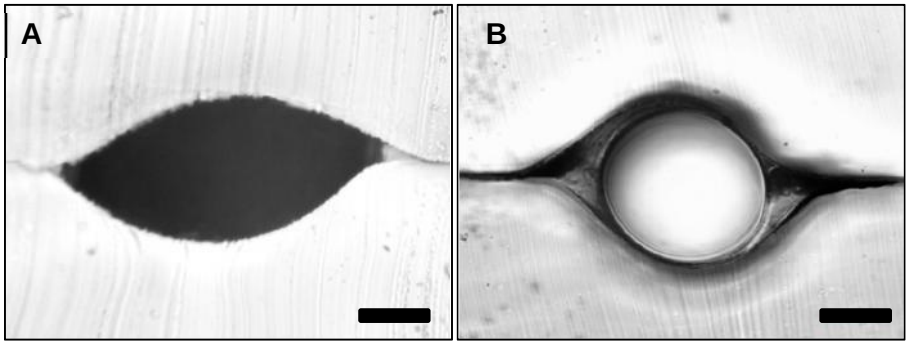

Figure 5.2 Optical microscope images of the cross-section of channels. (A) Cross-section of a channel around 200 µm in diameter prior to PDMS injection. (B) Post PDMS injection and curing procedure. Scale bar = 100 µm.

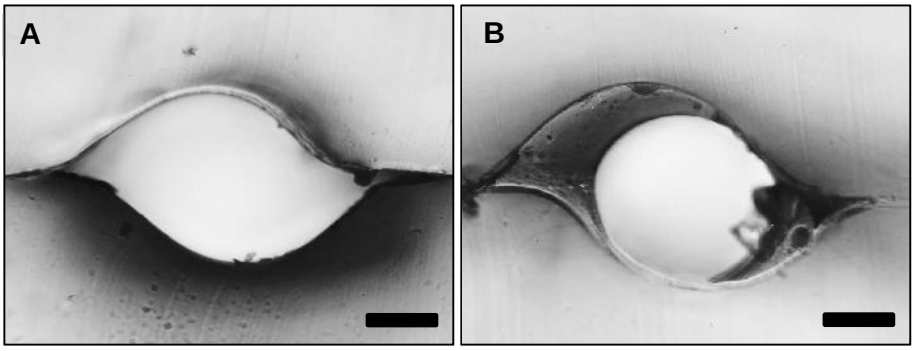

Figure 5.3 Optical microscope images of the cross-section of misaligned channels. (A) Cross-section of misaligned channel prior to PDMS injection. (B) Post PDMS injection and curing procedure. Misaligned channel resulted in correction by the PDMS injection. Scale bar = 100 µm.

Here the channels were perfectly circular as desired. The PDMS injection coating also allowed us to correct misaligned channels (Figure 5.3A). This misalignment can be present for various reasons; however, the PDMS injection coating mitigated the problem significantly (Figure 5.3B). Scanning electron micrograph (SEM) of the cross section of a circular channel is shown in Figure 5.4. This figure shows that a perfect circular channel was created after PDMS injection and all misalignments were corrected.

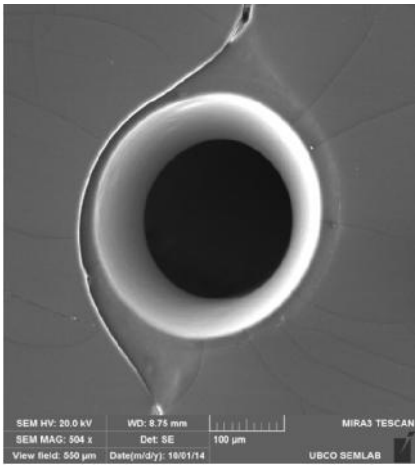

Figure 5.4 Scanning electron micrograph of the cross section of a circular channel.

In this microfluidic chip, two different phases of liquids are pumped into the center channel (water phase) and the outer channels (oil phase). The fluids meet at the cross-junction where the viscous force of the continuous oil phase flow overcomes the surface tension of water phase flow, which causes water droplets to be created. The cross-junction is a critical portion of this flow-focusing microfluidic chip. Figure 5.5 demonstrated that the cross-junction was not affected by liquid PDMS coating to form circular channels. As shown in Figure 5.6, the droplet generation was successful, and fluid flowed smoothly with no trace of blockage or leakage. Hydrogel droplets of different size were achieved through this process.

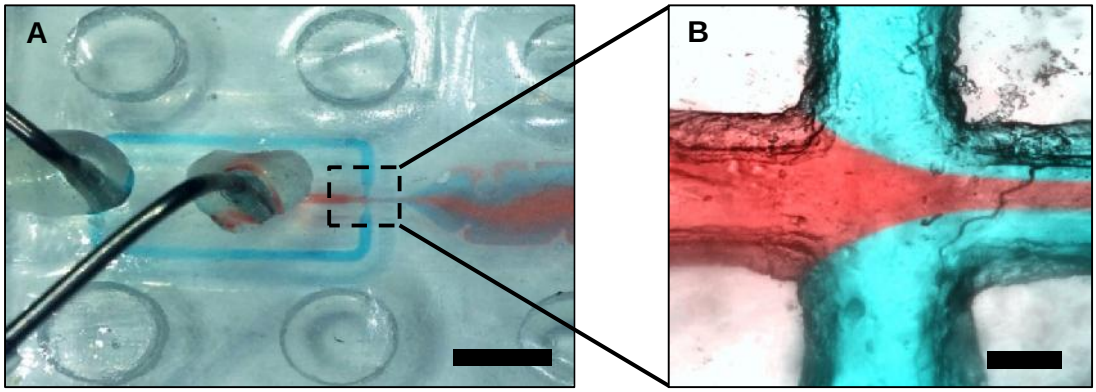

Figure 5.5 Junction of microfluidic chip after PDMS injection. (A) Different colored channels show clearly that there is no blockage of the junction during PDMS injection and circular channel formation. Scale bar = 5 mm. (B) an optical microscopic image shows the detail of the junction. Scale bar = 100 µm

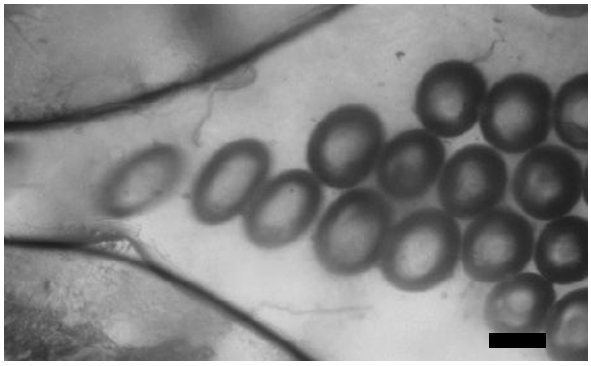

Figure 5.6 Droplet generation from the Microfluidic chip. Scale bar=200 µm

The 3D printed mold is a relatively simple manufacturing process to fabricate microfluidic channel devices. The 3D printing technique has advantages to rapidly fabricate complex structures with high aspect ratio comparing with the conventional photolithography technique which requires photomasks and a series of microfabrication process. Although the current resolution of 3D printers has a limitation to fabricate structures with hundreds of micrometers, in combination with the PDMS injection technique, 3D printed molds will be a promising solution to provide the flexibility to

fabricate various sizes of circular channels using the replica-molding softlithography technique. Therefore, the developed fabrication method using 3D printed molds can overcome the size limitation of microfluidic channel and will facilitate to use the 3D printing technique for fabricating a variety of microfluidic channel devices. For future work, this rapid fabricated device will be used to encapsulate cells to generate injectable microscale tissues and has many potential applications in biomedical engineering area.

5.4 Summary

In this chapter, a simple and low cost fabrication method is proposed for microfluidic droplet generators with circular channels. The PDMS channels were successfully cured and peeled off the 3D printed molds, and challenges regarding the interference of the 3D printed material as well as the cloudy (and rough 3D printed) surface finishes were addressed. Moreover, to create fully circular channels, and address challenges regarding the misalignment of the upper and lower halves, a PDMS injection coating method was utilized and optimized. The channels were successfully fabricated, and a flow-focusing microfluidic device for creating microgel droplets was assembled. No leakage was observed, and due to the use of circular channels, the device successfully created droplets of different size without blockage. The developed methodology provides a simple and effective way of fabricating circular microfluidic channels for numerous biological and chemical applications.

Chapter 6 Conclusion and Future works

6.1 Summary of Remarkable Results

Microfluidics flow-focusing devices are a promising platform for generating microgels that can be widely used in various applications such as tissue engineering, drug delivery, and cosmetic. In the tissue engineering application, cells are encapsulated in the microgels to produce injectable microscale tissues and study the effect of microenvironment on cell behaviors and cell-cell interactions. Investigating the effect of various parameters on droplet generation and optimizing these parameters are important to fabricate well-controlled cell-laden microgels.

In this thesis project, microfluidic flow-focusing devices were designed and fabricated. The conventional replica molding method using a microfabricated mold was adopted to fabricate the flow-focusing device. The physics of hydrogel pre-polymer droplet generation mechanism was computationally studied in three different regimes (i.e., squeezing, dripping, and jetting) and compared with previous results mostly discussing water droplet generation. In a squeezing regime, the droplets are usually created due to hydrodynamic pressure, while the dripping regime is due to the viscous drag force of continuous phase and the jetting regime is due to Rayleigh-Plateau instability. With the computational simulation, it was found that the concentration of GelMA dramatically affected the viscosity of pre-polymer solution and creation of droplets. GelMA pre-polymer droplets created with GelMA 8 wt% are bigger than GelMA 5 wt% at the same flow rate. The jetting regime observed due to the high viscosity and density of dispersed phase fluid, when GelMA 8 wt% was used as the dispersed phase at high flow rate of the continuous phase. It was found that increasing the flow rate ratio of the continuous phase and dispersed phase resulted in creating smaller droplets.

Using the fabricated flow-focusing devices, this study also experimentally investigated the effect of fluid properties, including viscosity, density, surface tension, and the flow rate of the dispersed and continuous phase for generating hydrogel pre-polymer droplets. GelMA pre-polymer solution with two different concentrations, 5 wt%, and 8 wt%, were used as the dispersed phase. Two different oils (i.e., hexadecane and light mineral oil) with 0 wt%, 5 wt%, and 20 wt% surfactants were used as the continuous phase. Experiments were conducted using different flow rates of continuous phase to study the influence of effective forces on droplet generation and optimize the hydrogel droplet generation. Three different regimes were investigated experimentally and compared with computational simulation results. All the results were summarized in two none dimensional numbers, $Ca_{c,}$ and Ca_{d}, to determine the range of the squeezing, dripping, and jetting regimes in a flow-focusing device for hydrogel droplets and shown in the phase diagram.

The presented phase diagram demonstrated that the range of capillary numbers created different regimes for generating GelMA pre-polymer droplets. It was found that at higher capillary numbers of GelMA pre-polymer solution droplets cannot be created because of the viscosity of the pre-polymer solution and resulted in the jetting regime, while water droplets could be created in the same condition based on the result of previous researches. Therefor, the phase diagram of water in the oil droplet generation from previous researchers is not helpful for hydrogel pre-polymer droplet generation because of the difference in viscosity and density between hydrogel and water.

The optimized parameters for GelMA pre-polymer droplet generation were used to encapsulate cells in GelMA microgels. By controlling the flow rate of the two phases, the type of oil, and the concentration of surfactant, the droplet size of the phase with different GelMA concentrations can be manipulated between 30 µm to 250 µm, which will be very

useful to control further the number of encapsulated cells and their surrounding microenvironment. MCF-7 breast cancer cells and 3T3 fibroblasts were encapsulated in the GelMA microgels and high cell viability >80% demonstrated that the flow-focusing system for generating GelMA pre-polymer droplets was a promising platform to fabricate cell-laden microgels for tissue engineering applications.

In addition to the microfabricated rectangular channel devices, a new method to fabricate circular channels has been introduced since the microfabrication method for the mold fabrication has limitations to fabricate only rectangular shape channels. With advantages of generating more uniform droplets using circular channels due to the uniform velocity profile produced in the circular channel cross section, the new method has been developed using 3D printed molds for upper and lower halves. To create fully circular channels, and address challenges regarding the misalignment of the upper and lower halves, a PDMS injection coating method was utilized and optimized. The channels were successfully fabricated, and the device generated hydrogel pre-polymer droplets. The developed methodology provides a simple and effective way of fabricating circular microfluidic channels for numerous biological and chemical applications.

6.2 Future works

There are several future works that are suggested in this thesis to improve the flow-focusing droplet generation system.

- Improve the method of separating the GelMA microgels from the continuous phase fluid (oil and surfactant): This study used a centrifugation method to filter oil out from the microgels. The process required several repetitions of centrifugation and re-suspending the microgels in PBS solution, resulting in losing many microgels during the process. For the future work, an addition of filtering chamber to the flow-focusing devices will help solve the problem of losing

microgels during the oil filtration process. The proposed design of filtering chamber is given in Figure 6.1. There are two inlets and two outlets. In the inlet 2, the microgel droplets with oil are injected into the filtering chamber, while PBS is injected into the inlet 1 with a higher flow rate to wash the oil out on the microgels. Then the microgels with PBS are coming out from the outlet 1, while the oil and surfactant are coming out from the outlet 2.

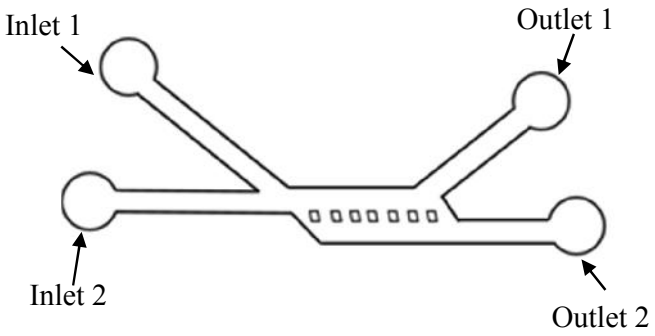

Figure 6.1 Schematic of filtering microfluidic device

- Improve cell viability: Using the UV light with low intensity, the crosslinking takes longer than 5 min which may cause harmful effects on cells. Our lab recently developed an ultrafast photocrosslinking method (< 1 min) using a laser diode. The laser-based method can be also applied to reduce the crosslinking time and increase the cell viability further.

Even distribution of cells: Evenly distributing cells in each droplet is currently difficult since cells tend to aggregate over time. Accordingly, cell numbers in droplets created in the flow focusing device were not controlled. For the future work, a microfluidic mixer can be added to the system to mix evenly cells with the hydrogel pre-polymer solution during the entire experimental process. A magnet mixer can be also used to mix the cells

in a syringe right before injecting into the tubing. Our lab is planning to place a small magnetic stirring bar inside the syringe and we will be able to mix the cells evenly by string the magnetic bar using a magnet rotor. In addition, a dielectrophoresis method can be also adapted to sort out droplets with and without cells [114][115][116].

References

[1] R.Lanza, R. Langer, J. P. Vacanti, eds. “Principles of tissue engineering.” *Academic Press*., 2000.

[2] N. Pallua, Ch. Suschek, eds. " Tissue Engineering: From lab to clinic.". *Springer Science & Business Media*, 2010.

[3] T. M. Chang, “Semipermeable Microcapsules.,” *Science*, vol. 146, no. 3643, pp. 524–525, 1964.

[4] A. Khademhosseini, R. Langer, J. Borenstein, and J. P. Vacanti, “Microscale technologies for tissue engineering and biology.,” *Proc. Natl. Acad. Sci. U. S. A.*, vol. 103, no. 8, pp. 2480–7, Feb. 2006.

[5] Y. Ikada, “Challenges in tissue engineering.,” *J. R. Soc. Interface*, vol. 3, no. 10, pp. 589–601, 2006.

[6] A. Khademhosseini and R. Langer, “Microengineered hydrogels for tissue engineering.,” *Biomaterials*, vol. 28, no. 34, pp. 5087–92, Dec. 2007.

[7] H. R. Nejad, E. Samiei, A. Ahmadi, and M. Hoorfar, “Gravity-driven hydrodynamic particle separation in digital microfluidic systems,” *RSC Adv.*, vol. 5, no. 45, pp. 35966–35975, 2015.

[8] Š. Selimović, J. Oh, H. Bae, M. Dokmeci, and A. Khademhosseini, “Microscale strategies for generating cell-encapsulating hydrogels,” *Polymers (Basel).*, vol. 4, no. 3, pp. 1554–1579, 2012.

[9] Z. Wang, R. Abdulla, B. Parker, and R. Samanipour, “A simple and high-resolution stereolithography-based 3D bioprinting system using visible light crosslinkable bioinks,” *Biofabrication*, vol. 7, no. 4, pp. 1–29, 2015.

[10] Z. Nie, M. Seo, S. Xu, P. C. Lewis, M. Mok, E. Kumacheva, G. M. Whitesides, P. Garstecki, and H. A. Stone, “Emulsification in a microfluidic flow-focusing

device: Effect of the viscosities of the liquids," *Microfluid. Nanofluidics*, vol. 5, pp. 585–594, 2008.

[11] E. Engel, A. Michiardi, M. Navarro, D. Lacroix, and J. a. Planell, "Nanotechnology in regenerative medicine: the materials side," *Trends Biotechnol.*, vol. 26, no. 1, pp. 39–47, 2008.

[12] J. W. Nichol and A. Khademhosseini, "Modular tissue engineering: engineering biological tissues from the bottom up," *Soft Matter*, vol. 5, no. 7, p. 1312, 2009.

[13] A. P. McGuigan and M. V Sefton, "Design and fabrication of sub-mm-sized modules containing encapsulated cells for modular tissue engineering," *Tissue Eng.*, vol. 13, no. 5, pp. 1069–1078, 2007.

[14] R. Dai, Z. Wang, R. Samanipour, K. Koo, and K. Kim, "Adipose-derived stem cells for tissue engineering and regenerative medicine applications," *Stem Cells Int.*, vol. 2016, 2016.

[15] E. Tumarkin, L. Tzadu, E. Csaszar, M. Seo, H. Zhang, A. Lee, R. Peerani, K. Purpura, P. W. Zandstra, and E. Kumacheva, "High-throughput combinatorial cell co-culture using microfluidics.," *Integr. Biol. (Camb).*, vol. 3, no. 6, pp. 653–662, 2011.

[16] A. Pathak and S. Kumar, "Biophysical regulation of tumor cell invasion: moving beyond matrix stiffness.," *Integr. Biol. (Camb).*, vol. 3, no. 4, pp. 267–278, 2011.

[17] A. Atala, R. Lanza, J. A. Thomson, and R. Nerem, *Principles of regenerative medicine*. Academic Press, 2010.

[18] J. Wan, "Microfluidic-based synthesis of hydrogel particles for cell microencapsulation and cell-based drug delivery," *Polymers (Basel).*, vol. 4, no. 2, pp. 1084–1108, 2012.

[19] L. Brannon-Peppas and R. S. Harland, *Absorbent polymer technology*. Elsevier,

2012.

[20] B. Balakrishnan and R. Banerjee, “Biopolymer-based hydrogels for cartilage tissue engineering,” *Chem. Rev.*, vol. 111, no. 8, pp. 4453–4474, 2011.

[21] H. Zimmermann, F. Ehrhart, D. Zimmermann, K. Müller, A. Katsen-Globa, M. Behringer, P. J. Feilen, P. Gessner, G. Zimmermann, and S. G. Shirley, “Hydrogel-based encapsulation of biological, functional tissue: fundamentals, technologies and applications,” *Appl. Phys. A*, vol. 89, no. 4, pp. 909–922, 2007.

[22] J. L. Drury and D. J. Mooney, “Hydrogels for tissue engineering: scaffold design variables and applications,” *Biomaterials*, vol. 24, no. 24, pp. 4337–4351, Nov. 2003.

[23] B. V Slaughter, S. S. Khurshid, O. Z. Fisher, A. Khademhosseini, and N. A. Peppas, “Hydrogels in regenerative medicine,” *Adv Mater*, vol. 21, no. 32–33, pp. 3307–3329, 2009.

[24] J. Thiele, Y. Ma, S. M. C. Bruekers, S. Ma, and W. T. S. Huck, “25th anniversary article: Designer hydrogels for cell cultures: A materials selection guide,” *Adv. Mater.*, vol. 26, no. 1, pp. 125–148, 2014.

[25] A. Kang, J. Park, J. Ju, G. S. Jeong, and S. H. Lee, “Cell encapsulation via microtechnologies,” *Biomaterials*, vol. 35, no. 9, pp. 2651–2663, 2014.

[26] S. Li, I. Molina, M. Bueno Martinez, and M. Vert, “Hydrolytic and enzymatic degradations of physically crosslinked hydrogels prepared from PLA/PEO/PLA triblock copolymers,” *J. Mater. Sci. Mater. Med.*, vol. 13, no. 1, pp. 81–86, 2002.

[27] S. G. Lévesque and M. S. Shoichet, “Synthesis of enzyme-degradable, peptide-cross-linked dextran hydrogels,” *Bioconjug. Chem.*, vol. 18, no. 3, pp. 874–885, 2007.

[28] K. Y. Lee, K. H. Bouhadir, and D. J. Mooney, “Controlled degradation of

hydrogels using multi-functional cross-linking molecules," *Biomaterials*, vol. 25, no. 13, pp. 2461–2466, 2004.

[29] T. Nisisako, T. Torii, and T. Higuchi, "Droplet formation in a microchannel network.," *Lab Chip*, vol. 2, pp. 24–26, 2002.

[30] S. L. Anna and H. C. Mayer, "Microscale tipstreaming in a microfluidic flow focusing device," *Phys. Fluids*, vol. 18, 2006.

[31] A. S. Utada, A. Fernandez-Nieves, H. a. Stone, and D. a. Weitz, "Dripping to jetting transitions in coflowing liquid streams," *Phys. Rev. Lett.*, vol. 99, no. August, pp. 1–4, 2007.

[32] L. Y. Chu, A. S. Utada, R. K. Shah, J. W. Kim, and D. a. Weitz, "Controllable monodisperse multiple emulsions," *Angew. Chemie - Int. Ed.*, vol. 46, no. 47, pp. 8970–8974, 2007.

[33] S. Okushima, T. Nisisako, T. Torii, and T. Higuchi, "Controlled production of monodisperse double emulsions by two-step droplet breakup in microfluidic devices," *Langmuir*, vol. 20, no. 23, pp. 9905–9908, 2004.

[34] R. Seemann, M. Brinkmann, T. Pfohl, and S. Herminghaus, "Droplet based microfluidics," *Reports Prog. Phys.*, vol. 75, no. 1, p. 016601, 2011.

[35] E. Tumarkin, L. Tzadu, E. Csaszar, M. Seo, H. Zhang, A. Lee, R. Peerani, K. Purpura, P. W. Zandstra, and E. Kumacheva, "High-throughput combinatorial cell co-culture using microfluidics," *Integr. Biol.*, vol. 3, no. 6, p. 653, 2011.

[36] J. Clausell-Tormos, D. Lieber, J. C. Baret, A. El-Harrak, O. J. Miller, L. Frenz, J. Blouwolff, K. J. Humphry, S. Köster, H. Duan, C. Holtze, D. a. Weitz, A. D. Griffiths, and C. a. Merten, "Droplet-Based Microfluidic Platforms for the Encapsulation and Screening of Mammalian Cells and Multicellular Organisms," *Chem. Biol.*, vol. 15, no. 5, pp. 427–437, 2008.

[37] W. H. Tan and S. Takeuchi, “Monodisperse alginate hydrogel microbeads for cell encapsulation,” *Adv. Mater.*, vol. 19, no. 18, pp. 2696–2701, 2007.

[38] J. H. Xu, P. F. Dong, H. Zhao, C. P. Tostado, and G. S. Luo, “The Dynamic Effects of Surfactants on Droplet Formation in Coaxial Microfluidic Devices,” *Langmuir*, 2012.

[39] A. Kumachev, J. Greener, E. Tumarkin, E. Eiser, P. W. Zandstra, and E. Kumacheva, “High-throughput generation of hydrogel microbeads with varying elasticity for cell encapsulation,” *Biomaterials*, vol. 32, no. 6, pp. 1477–1483, 2011.

[40] E. Um, D.-S. Lee, H.-B. Pyo, and J.-K. Park, “Continuous generation of hydrogel beads and encapsulation of biological materials using a microfluidic droplet-merging channel,” *Microfluid. Nanofluidics*, vol. 5, no. 4, pp. 541–549, Feb. 2008.

[41] C.-H. Choi, J.-H. Jung, Y. W. Rhee, D.-P. Kim, S.-E. Shim, and C.-S. Lee, “Generation of monodisperse alginate microbeads and in situ encapsulation of cell in microfluidic device,” *Biomed. Microdevices*, vol. 9, no. 6, pp. 855–862, 2007.

[42] S. Sugiura, T. Oda, Y. Izumida, Y. Aoyagi, M. Satake, A. Ochiai, N. Ohkohchi, and M. Nakajima, “Size control of calcium alginate beads containing living cells using micro-nozzle array,” *Biomaterials*, vol. 26, no. 16, pp. 3327–3331, 2005.

[43] S. Sugiura, T. Oda, Y. Aoyagi, R. Matsuo, T. Enomoto, K. Matsumoto, T. Nakamura, M. Satake, A. Ochiai, N. Ohkohchi, and M. Nakajima, “Microfabricated airflow nozzle for microencapsulation of living cells into 150 micrometer microcapsules,” *Biomed. Microdevices*, vol. 9, no. 1, pp. 91–99, 2007.

[44] T. Cubaud and T. G. Mason, “Capillary threads and viscous droplets in square microchannels,” *Phys. Fluids*, vol. 20, pp. 1–11, 2008.

[45] L. Peng, M. Yang, S. Guo, W. Liu, and X. Zhao, “The effect of interfacial tension

on droplet formation in flow-focusing microfluidic device.," *Biomed. Microdevices*, vol. 13, pp. 559–564, 2011.

[46] B. Dollet, W. Van Hoeve, J. P. Raven, P. Marmottant, and M. Versluis, "Role of the channel geometry on the bubble pinch-off in flow-focusing devices," *Phys. Rev. Lett.*, vol. 100, no. JANUARY, pp. 1–4, 2008.

[47] K. J. Humphry, A. Ajdari, A. Fernández-Nieves, H. A. Stone, and D. A. Weitz, "Suppression of instabilities in multiphase flow by geometric confinement," *Phys. Rev. E - Stat. Nonlinear, Soft Matter Phys.*, vol. 79, pp. 1–5, 2009.

[48] T. Ward, M. Faivre, M. Abkarian, and H. A. Stone, "Microfluidic flow focusing: Drop size and scaling in pressure versus flow-rate-driven pumping," *Electrophoresis*, vol. 26, pp. 3716–3724, 2005.

[49] C. H. Chen, A. R. Abate, D. Lee, E. M. Terentjev, and D. A. Weitz, "Microfluidic assembly of magnetic hydrogel particles with uniformly anisotropic structure," *Adv. Mater.*, vol. 21, no. 31, pp. 3201–3204, 2009.

[50] T. Aikawa, T. Konno, M. Takai, and K. Ishihara, "Spherical phospholipid polymer hydrogels for cell encapsulation prepared with a flow-focusing microfluidic channel device," *Langmuir*, vol. 28, pp. 2145–2150, 2012.

[51] T.-D. Dang, Y. H. Kim, H. G. Kim, and G. M. Kim, "Preparation of monodisperse PEG hydrogel microparticles using a microfluidic flow-focusing device," *J. Ind. Eng. Chem.*, vol. 18, no. 4, pp. 1308–1313, Jul. 2012.

[52] J. Jung and J. Oh, "Cell-induced flow-focusing instability in gelatin methacrylate microdroplet generation.," *Biomicrofluidics*, vol. 8, no. 3, p. 036503, 2014.

[53] S. R. Shin, B. Aghaei-Ghareh-Bolagh, T. T. Dang, S. N. Topkaya, X. Gao, S. Y. Yang, S. M. Jung, J. H. Oh, M. R. Dokmeci, X. Tang, and A. Khademhosseini, "Cell-laden microengineered and mechanically tunable hybrid hydrogels of gelatin

and graphene oxide," *Adv. Mater.*, vol. 25, pp. 6385–6391, 2013.

[54] J. F. Edd, D. Di Carlo, K. J. Humphry, S. Köster, D. Irimia, D. a Weitz, and M. Toner, "Controlled encapsulation of single-cells into monodisperse picolitre drops.," *Lab Chip*, vol. 8, no. 8, pp. 1262–1264, 2008.

[55] C. Kim, K. S. Lee, Y. E. Kim, K.-J. Lee, S. H. Lee, T. S. Kim, and J. Y. Kang, "Rapid exchange of oil-phase in microencapsulation chip to enhance cell viability.," *Lab Chip*, vol. 9, no. 9, pp. 1294–1297, 2009.

[56] C. Kim, S. Chung, Y. E. Kim, K. S. Lee, S. H. Lee, K. W. Oh, and J. Y. Kang, "Generation of core-shell microcapsules with three-dimensional focusing device for efficient formation of cell spheroid.," *Lab Chip*, vol. 11, no. 2, pp. 246–252, 2011.

[57] L. Wu, P. Chen, Y. Dong, X. Feng, and B. F. Liu, "Encapsulation of single cells on a microfluidic device integrating droplet generation with fluorescence-activated droplet sorting," *Biomed. Microdevices*, vol. 15, no. 3, pp. 553–560, 2013.

[58] L. Capretto, S. Mazzitelli, G. Luca, and C. Nastruzzi, "Preparation and characterization of polysaccharidic microbeads by a microfluidic technique: Application to the encapsulation of Sertoli cells," *Acta Biomater.*, vol. 6, no. 2, pp. 429–435, 2010.

[59] S. Köster, F. E. Angilè, H. Duan, J. J. Agresti, A. Wintner, C. Schmitz, A. C. Rowat, C. a Merten, D. Pisignano, A. D. Griffiths, and D. a Weitz, "Drop-based microfluidic devices for encapsulation of single cells.," *Lab Chip*, vol. 8, no. 7, pp. 1110–1115, 2008.

[60] Y. T. Matsunaga, Y. Morimoto, and S. Takeuchi, "Molding cell beads for rapid construction of macroscopic 3D tissue architecture," *Adv. Mater.*, vol. 23, no. 12, pp. 90–94, 2011.

[61] M. J. Jensen, H. A. Stone, and H. Bruus, “A numerical study of two-phase Stokes flow in an axisymmetric flow-focusing device,” *Phys. Fluids*, vol. 18, no. 2006, 2006.

[62] M. M. Dupin, I. Halliday, and C. M. Care, “Simulation of a microfluidic flow-focusing device,” *Phys. Rev. E - Stat. Nonlinear, Soft Matter Phys.*, vol. 73, pp. 1–4, 2006.

[63] C. Zhou, P. Yue, and J. J. Feng, “Formation of simple and compound drops in microfluidic devices,” *Phys. Fluids*, vol. 18, no. 2006, 2006.

[64] Y. Shi, G. H. Tang, and H. H. Xia, “Lattice Boltzmann simulation of droplet formation in T-junction and flow focusing devices,” *Comput. Fluids*, vol. 90, pp. 155–163, 2014.

[65] A. Gupta, H. S. Matharoo, D. Makkar, and R. Kumar, “Droplet formation via squeezing mechanism in a microfluidic flow-focusing device,” *Comput. Fluids*, vol. 100, pp. 218–226, 2014.

[66] W. Lee, L. M. Walker, and S. L. Anna, “Role of geometry and fluid properties in droplet and thread formation processes in planar flow focusing,” *Phys. Fluids*, vol. 21, no. 3, pp. 1–15, 2009.

[67] R. Samanipour, M. Maerefat, and H. R. Nejad, “Numerical study of the effect of ultrasound frequency on temperature distribution in layered tissue,” *J. Therm. Biol.*, vol. 38, no. 6, pp. 287–293, 2013.

[68] J. Xu and D. Attinger, “Drop on demand in a microfluidic chip,” vol. 065020, 2009.

[69] B. G. Chung, K.-H. Lee, A. Khademhosseini, and S.-H. Lee, “Microfluidic fabrication of microengineered hydrogels and their application in tissue engineering,” *Lab Chip*, vol. 12, no. 1, p. 45, 2012.

[70] Z. Wang, R. Samanipour, K. Kyo-in, and K. Kim, "Organ-on-a-Chip Platforms for Drug Delivery and Cell Characterization: A Review," *Sensors Mater.*, vol. 27, no. 6, pp. 487–506, 2015.

[71] Z. Wang, R. Samanipour, and K. Kim, "Organ-on-a-Chip Platforms for Drug Screening and Tissue Engineering," in *Biomedical Engineering: Frontier Research and Converging Technologies*, Springer, 2016, pp. 209–233.

[72] H. Lee, M. Chung, and N. L. Jeon, "Microvasculature: An essential component for organ-on-chip systems," *MRS Bull.*, vol. 39, no. January, pp. 51–59, 2014.

[73] R. Voelkel, U. Vogler, A. Bich, P. Pernet, K. J. Weible, M. Hornung, R. Zoberbier, E. Cullmann, L. Stuerzebecher, and T. Harzendorf, "Advanced mask aligner lithography: new illumination system," *Opt. Express*, vol. 18, no. 20, pp. 20968–20978, 2010.

[74] D. Q. and G. M. W. Younan Xia, Joe Tien, "Non-Photolithographic Methods for Fabrication of Elastomeric for Use Stamps in Microcontact Printing," *Langmuir*, vol. 12, no. 16, pp. 4033–4038, 1996.

[75] C. Yang, W. Wang, and Z. Li, "Optimization of corona-triggered PDMS-PDMS bonding method," in *Proceedings of the 2009 4th IEEE International Conference of Nano/Micro Engineering and Molecular Systems*, 2009, pp. 319–322.

[76] S.-Y. Teh, R. Lin, L.-H. Hung, and A. P. Lee, "Droplet microfluidics.," *Lab Chip*, vol. 8, no. 2, pp. 198–220, 2008.

[77] a. S. Utada, L.-Y. Chu, a. Fernandez-Nieves, D. R. Link, C. Holtze, and D. a. Weitz, "Dripping, Jetting, Drops, and Wetting: The Magic of Microfluidics," *MRS Bull.*, vol. 32, no. 09, pp. 702–708, 2007.

[78] Y.-C. Tan, V. Cristini, and A. P. Lee, "Monodispersed microfluidic droplet generation by shear focusing microfluidic device," *Sensors Actuators B Chem.*,

vol. 114, no. 1, pp. 350–356, 2006.

[79] S. Sugiura, M. Nakajima, and M. Seki, “Effect of channel structure on microchannel emulsification,” *Langmuir*, vol. 18, no. 15, pp. 5708–5712, 2002.

[80] C. Cramer, P. Fischer, and E. J. Windhab, “Drop formation in a co-flowing ambient fluid,” *Chem. Eng. Sci.*, vol. 59, no. 15, pp. 3045–3058, 2004.

[81] P. Garstecki, H. A. Stone, and G. M. Whitesides, “Mechanism for flow-rate controlled breakup in confined geometries: A route to monodisperse emulsions,” *Phys. Rev. Lett.*, vol. 94, no. 16, p. 164501, 2005.

[82] J. K. Nunes, S. S. H. Tsai, J. Wan, and H. A. Stone, “Dripping and jetting in microfluidic multiphase flows applied to particle and fiber synthesis.,” *J. Phys. D. Appl. Phys.*, vol. 46, p. 114002, 2013.

[83] T. P. Lagus and J. F. Edd, “A review of the theory, methods and recent applications of high-throughput single-cell droplet microfluidics,” *J. Phys. D. Appl. Phys.*, vol. 46, p. 114005, 2013.

[84] P. Garstecki, H. a. Stone, and G. M. Whitesides, “Mechanism for Flow-Rate Controlled Breakup in Confined Geometries: A Route to Monodisperse Emulsions,” *Phys. Rev. Lett.*, vol. 94, no. 16, p. 164501, 2005.

[85] Z. Nie, M. Seo, S. Xu, P. C. Lewis, M. Mok, E. Kumacheva, G. M. Whitesides, P. Garstecki, and H. A. Stone, “Emulsification in a microfluidic flow-focusing device: effect of the viscosities of the liquids,” *Microfluid. Nanofluidics*, vol. 5, no. 5, pp. 585–594, 2008.

[86] J. K. Nunes, S. S. H. Tsai, J. Wan, and H. a Stone, “Dripping and jetting in microfluidic multiphase flows applied to particle and fibre synthesis,” *J. Phys. D. Appl. Phys.*, vol. 46, no. 11, p. 114002, Mar. 2013.

[87] R. Barnkob and M. B. Andersen, “Two Phase Flow by Level Set Method,” 2007.

[88] C. Cha, J. Oh, K. Kim, Y. Qiu, M. Joh, S. R. Shin, X. Wang, G. Camci-Unal, K. T. Wan, R. Liao, and A. Khademhosseini, "Microfluidics-assisted fabrication of gelatin-silica core-shell microgels for injectable tissue constructs," *Biomacromolecules*, vol. 15, no. 1, pp. 283–290, 2014.

[89] J. W. Nichol, S. Koshy, H. Bae, C. M. Hwang, and A. Khademhosseini, "NIH Public Access," vol. 31, no. 21, pp. 5536–5544, 2011.

[90] L. Rayleigh, "On the Capillary Phenomena of Jets," *Proc. R. Soc. London*, vol. 29, no. 1879, pp. 71–97, 1879.

[91] B. Y. J. N. Phillips, "THE ENERGETICS OF MICELLE FORMATION," no. i, 1954.

[92] a. R. Abate, a. Poitzsch, Y. Hwang, J. Lee, J. Czerwinska, and D. a. Weitz, "Impact of inlet channel geometry on microfluidic drop formation," *Phys. Rev. E - Stat. Nonlinear, Soft Matter Phys.*, vol. 80, no. 2, pp. 1–5, 2009.

[93] M. Alvarado-Velez, S. B. Pai, and R. V Bellamkonda, "Hydrogels as carriers for stem cell transplantation.," *IEEE Trans. Biomed. Eng.*, vol. 61, no. 5, pp. 1474–81, 2014.

[94] C. Limban, A. V. Missir, A. M. Grumezescu, A. E. Oprea, V. Grumezescu, B. Ștefan Vasile, G. Socol, R. Truşcă, M. T. Caproiu, and M. C. Chifiriuc, "Bioevaluation of Novel Anti-Biofilm Coatings Based on PVP/Fe3O4 Nanostructures and 2-((4-Ethylphenoxy) methyl)-N-(arylcarbamothioyl) benzamides," *Molecules*, vol. 19, no. 8, pp. 12011–12030, 2014.

[95] C.-H. Lin, G.-B. Lee, B.-W. Chang, and G.-L. Chang, "A new fabrication process for ultra-thick microfluidic microstructures utilizing SU-8 photoresist," *J. Micromechanics Microengineering*, vol. 12, no. 5, pp. 590–597, Sep. 2002.

[96] M. Abdelgawad, C. Wu, and W. Y. Chien, "A fast and simple method to fabricate

circular microchannels in polydimethylsiloxane (PDMS)," *Lab Chip*, vol. 11, no. 3, pp. 545–551, Feb. 2011.

[97] S. Takeuchi, P. Garstecki, D. B. Weibel, and G. M. Whitesides, "An Axisymmetric Flow-Focusing Microfluidic Device," *Adv. Mater.*, vol. 17, no. 8, pp. 1067–1072, Apr. 2005.

[98] R. H. Baughman, A. a Zakhidov, and W. a de Heer, "Carbon nanotubes--the route toward applications.," *Science*, vol. 297, no. 5582, pp. 787–92, Aug. 2002.

[99] A. Star, J. P. Gabriel, K. Bradley, and G. Gru, "Electronic Detection of Specific Protein Binding Using Nanotube FET Devices," 2003.

[100] B. R. Munson, D. F. Young, and T. H. Okiishi, *Fundamentals of fluid mechanics*. New York, 1990.

[101] E. Kang, S.-J. Shin, K. H. Lee, and S.-H. Lee, "Novel PDMS cylindrical channels that generate coaxial flow, and application to fabrication of microfibers and particles.," *Lab Chip*, vol. 10, no. 14, pp. 1856–61, Jul. 2010.

[102] A. Agarwal, N. Ranganathan, W.-L. Ong, K. C. Tang, and L. Yobas, "Self-sealed circular channels for micro-fluidics," *Sensors Actuators A Phys.*, vol. 142, no. 1, pp. 80–87, Mar. 2008.

[103] K. Lee, C. Kim, K. S. Shin, J. W. Lee, B.-K. Ju, T. S. Kim, S.-K. Lee, and J. Y. Kang, "Fabrication of round channels using the surface tension of PDMS and its application to a 3D serpentine mixer," *J. Micromechanics Microengineering*, vol. 17, no. 8, pp. 1533–1541, Aug. 2007.

[104] A. I. Shallan, P. Smejkal, M. Corban, R. M. Guijt, and M. C. Breadmore, "Cost-effective three-dimensional printing of visibly transparent microchips within minutes," *Anal. Chem.*, vol. 86, pp. 3124–3130, 2014.

[105] Z. Wang, R. Samanipour, and K. Kim, "The cleanroom-free rapid fabrication of a

liquid conductivity sensor for surface water quality monitoring," *Microsyst. Technol.*, pp. 1–6, 2015.

[106] P. Wu, Y. Wang, Z. Luo, Y. Li, M. Li, and L. He, "A 3D easily-assembled Micro-Cross for droplet generation.," *Lab Chip*, vol. 14, no. 4, pp. 795–8, Feb. 2014.

[107] T.-F. Hong, W.-J. Ju, M.-C. Wu, C.-H. Tai, C.-H. Tsai, and L.-M. Fu, "Rapid prototyping of PMMA microfluidic chips utilizing a CO2 laser," *Microfluid. Nanofluidics*, vol. 9, no. 6, pp. 1125–1133, May 2010.

[108] M. E. Wilson, N. Kota, Y. Kim, Y. Wang, D. B. Stolz, P. R. LeDuc, and O. B. Ozdoganlar, "Fabrication of circular microfluidic channels by combining mechanical micromilling and soft lithography," *Lab Chip*, vol. 11, no. 8, p. 1550, 2011.

[109] Z. Huang, X. Li, M. Martins-Green, and Y. Liu, "Microfabrication of cylindrical microfluidic channel networks for microvascular research," *Biomed. Microdevices*, vol. 14, no. 5, pp. 873–883, 2012.

[110] S. T. Beyer, A. Bsoul, K. Walus, and A. Ahmadi, "3D alginate contructs for tissue engineering printed using a coaxial flow focusing microfluidic device," in *2013 Transducers & Eurosensors XXVII*, 2013, no. June, pp. 1206–1209.

[111] A. Ahmadi, R. Samanipour, B. Parker, and K. Kim, "Rapid fabrication of circular channel microfluidic flow-focusing devices for hydrogel droplet generation," *Micro Nano Lett.*, vol. 11, no. 1, pp. 41–45, 2016.

[112] R. Udroiu and L. a Mihail, "Experimental determination of surface roughness of parts obtained by rapid prototyping," in *CSECS'09 Proceedings of the 8th WSEAS International Conference on Circuits, Systems, Electronics, Control & Signal Processing*, 2009, no. October, pp. 283–286.

[113] P. H. King, G. Jones, H. Morgan, M. R. R. de Planque, and K.-P. Zauner,

"Interdroplet bilayer arrays in millifluidic droplet traps from 3D-printed moulds.," *Lab Chip*, vol. 14, pp. 722–9, 2014.

[114] H. R. Nejad and M. Hoorfar, "Purification of a droplet using negative dielectrophoresis traps in digital microfluidics," *Microfluid. Nanofluidics*, vol. 18, no. 3, pp. 483–492, 2015.

[115] E. Samiei, H. Rezaei Nejad, and M. Hoorfar, "A dielectrophoretic-gravity driven particle focusing technique for digital microfluidic systems," *Appl. Phys. Lett.*, vol. 106, no. 20, p. 204101, May 2015.

[116] H. R. Nejad, O. Z. Chowdhury, M. D. Buat, and M. Hoorfar, "Characterization of the geometry of negative dielectrophoresis traps for particle immobilization in digital microfluidic platforms.," *Lab Chip*, vol. 13, no. 9, pp. 1823–30, 2013.

[117] L. L. F. Agostinho, G. Tamminga, C. U. Yurteri, S. P. Brouwer, E. C. Fuchs, and J. C. M. Marijnissen, "Morphology of water electrosprays in the simple-jet mode," *Phys. Rev. E*, vol. 86, no. 6, p. 66317, 2012.

[118] M. Seo, C. Paquet, Z. Nie, S. Xu, and E. Kumacheva, "Microfluidic consecutive flow-focusing droplet generators," *Soft Matter*, vol. 3, no. 8, pp. 986–992, 2007.

[119] M. Sun, S. S. Bithi, and S. a Vanapalli, "Microfluidic static droplet arrays with tuneable gradients in material composition.," *Lab Chip*, vol. 11, no. 23, pp. 3949–52, Dec. 2011.

[120] C. a Stan, S. K. Y. Tang, and G. M. Whitesides, "Independent control of drop size and velocity in microfluidic flow-focusing generators using variable temperature and flow rate.," *Anal. Chem.*, vol. 81, no. 6, pp. 2399–402, 2009.